10

Distributed Generation and Islanding – Study on Converter Modeling of PV Grid-Connected Systems under Islanding Phenomena

N. Chayawatto[1], N.Patcharaprakiti[2], V. Monyakul[1],
K.Kirtikara[1] and K. Tunlasakun[1]
Clean Energy Systems Group (CES),
King Mongkut's University of Technology Thonburi (KMUTT) [1],
Bangkok 10140, Thailand
Rajamangala University of Technology Lanna[2] , Chiang Mai, Thailand
Corresponding author: V. Monyakul <v_monyakul@yahoo.com>

Abstract

Thailand government has launched a 15-year (2008-2022) strategic plan on new and renewable energy. Possible electricity generated from solar photovoltaic has been estimated with a potential of 50,000 MW, whereas at present the cumulative installed wattage is only 32 MW. Under the Plan, numbers of measures and incentives are provided for participation of private very small power producers (VSPP) generating and selling the electricity into the utilities. Most VSPPs generate electricity from renewable sources such as mini-hydro, biogas and biomass, wind and solar. Examples of measures and incentives are the Renewable Portfolio Standard (RPS) for the generating utility and independent power producers (IPP), a feed in tariff with an extra adder, soft loans and tax reduction.

The past decade in Thailand has seen shifts from PV used in the public market through government demonstration projects to the consumer market, installations of PV VSPPs and domestic roof-top grid connected PV units gain momentum. With the government incentive more households will be attracted to produce electricity from solar PV and wind energy. As domestic roof sizes are limited, PV roof-top grid-connected units will be of small capacity, less than 10 kW. It is this possible large expansion of market for thousands of small PV roof-top grid-connected units or wind systems in Thailand, and eastern Asia, that draws our attention to the study of single phase distributed generator grid-connected systems. Our focus will be on the anti-islanding protection, which is of concerns to Thai electrical utilities. In order to know the behavior and the effect of anti-islanding techniques, the converter modeling of PV grid-connected systems under islanding phenomena is studied. The approach of modeling is to model a dc-ac full bridge switching converter PV grid-connected system under islanding phenomena using two mathematical modeling techniques. One corresponds to a state-space averaging technique (no linearization) and the other a piecewise technique. The former technique applies a state-space averaging technique (no-

linearization) and voltage source inverter with current control as "large signal modeling". The latter one employs piecewise functions. Each piecewise function ON and OFF interval are derived by using a state-space equation and solved by the Laplace Transform technique. Both are used to analyze the dynamic response of load voltages under 3 different resistive loads, i.e, 125%, 100% and 25% of inverter output and a RLC load when the grid system is disconnected. An experiment on islanding detections is set up. The equations from two proposed modeling technique are handled by MATLAB/SIMULINK software. The results of the proposed models are compared with experiments and the PSpice simulation showing good agreement. It is found that the proposed models consumes much less computation time than the PSpice Program and does not encounter any convergence problem. For islanding trip times, it is found that in all cases tested they are about 2-3 cycles or 40-60 ms, passing the criteria of regulations and standards of the electric utilities of Thailand.
This technique can potentially be further developed for implementation in larger systems consisting of a large array of grid-connected PV modules or other distributed generators.

1.Introduction

1.1 Renewable Energy and Electricity Generation in Thailand

In 2007, the Thailand government launched a strategic 15- year plan for promotion of the renewable energy technology with the goal of increase uses of renewable energy from 5.8% at present to 20% of final energy consumption [1]. The renewable energy targets, covering solar, wind, hydro, wastes, hydrogen, various types of biomasses and biofuels, are outlined in Table 1, expressed as electricity power generation and ktoe. In terms of electrical power generated, the electrical power from solar PV, wind, biomass, biogas, garbage and hydrogen will increase from the existing 1,714 MW to 5,508 MW equivalent to 2,990 ktoe, the thermal energy from renewable energy sources from 3,007 ktoe to 7,433 ktoe, and the biomass energy from less than 10 ktoe to 3,986 ktoe..

Fuel	Potential	Existing	2007-2011		2012-2016		2017-2022	
Electricity	**MW**	**MW**	**MW**	**ktoe**	**MW**	**ktoe**	**MW**	**ktoe**
Solar PV	**50,000**	**32**	**55**	**6**	**95**	**11**	**500**	**55**
Wind	1,600	1	115	13	375	42	800	89
Hydro	700	56	165	43	281	73	324	85
Biomass	400	1,610	2,800	1,463	3,220	1,682	3,700	1,933
Biogas	190	46	60	27	90	40	120	54
Garbage	400	5	78	35	130	58	160	72
Hydrogen	-		0	0	0	0	3.5	1
Total Electricity		1,750	3,273	1,587	4,191	1,907	5,608	2,990
Thermal Energy	Ktoe	ktoe		ktoe		ktoe		ktoe
Solar Thermal	154	1		5		17.5		38
Biomass	7,400	2,781		3,660		5,000		6,760
Biogas	600	224		470		540		600
Garbage		1		15		24		35

Total Thermal		3,007		4,150		5,528		7,433
BioEnergy	Ml/day	ktoe	Ml/day	ktoe	Ml/day	ktoe	Ml/day	ktoe
Ethanol	3.00	1.24	3.00	805	6.20	1,686	9.00	2,447
Biodiesel	4.20	1.56	3.00	950	3.64	1,145	4.50	1,415
Hydrogen			0	0	0	0	$0.1x10^6$ kg	124
Total Bioenergy			6.00	1,755	9.84	2,831	13.50	3,986

Table 1 Potential Renewable Energy and 15 –Year Plan of Thailand

The Plan is divided into 3 periods, the Short Term, the Mid Term and the Long Term. Its essences are

1) The Short Term (2007-2011) : The first stage will concentrate on promoting proven technologies and high potential renewable energy such as bio-energy biomass, biogas and compressed natural gas.

2) The Mid Term (2012-2017) : Renewable energy industries will be promoted with supports on research and development on ethanol production, biodiesel from algae, oil production from biomass, and hydrogen generation. It is envisaged that a "green city" demonstration will be carried out and applications of renewable energy to community levels strengthened.

3) The Long Term (2017-2022) : Hydrogen economy, the green city and renewable energy in community will be expanded. Thailand would lead as an energy leader in bioenergy and renewable energy of ASEAN.

Among many renewable energy sources of significant, solar PV has a very high potential, estimated to about 50,000 MW. The daily average of solar radiation in Thailand is about 5.0 to 5.3 kWh/m^2-day, corresponding to 18 to19 MJ/m^2-day. High values 20-24 MJ/m^2-day are recorded during April and May. The north eastern and northern regions receive about 2,200 to 2,900 hours of sunshine on annual basis, 6-8 sunshine-hours per day. However, the exiting PV power generation is only 32 MW.

Thailand electricity sector of the country can be divided into generation, transmission and distribution sectors. In the past, it was dominated by 3 state enterprise utilities. They are one generation and transmission utility, the Electricity Generating Authority of Thailand-EGAT, ,and two distribution utilities, the Provincial Electricity Authority-PEA and the Metropolitan Electricity Authority-MEA. The industry was liberalized in early 1990s allowing participation of the private sector in power generation. Presently in the generation sector, two major power generators are EGAT 48% and 39 % from private independent power producers- IPPs, with generating capacity more than 90 MW, initiated in early 1990s. 3% are imported from neighboring Laos. The remaining are from small power producers- SPP, generating capacity l0-90 MW, and very small power producers – VSPP, less than 10 MW. SPPs use mainly biomass whereas VSPPs are mostly mini hydroelectric, wind and solar PV. Electricity generated by EGAT, and IPPs are transmitted through the network of EGAT to the 2 distributors, PEA and MEA. SPPs directly sell power to users, mainly large industries, some are connected to PEA and MEA. The structure of electricity industry of Thailand is shown as Fig.1.

It should be noted that electricity generated by renewable energy sources will be SPPs and VSPPs. They will become more common as renewable energy promotion expanded, hundreds or thousands of them can be connected to the distribution network in the future. The 3 utilities, EGAT, PEA and MEA are concerned on power electrical quality resulting from connecting of large numbers of grid-connected SPPs and VSPPs, being distributed in nature, to the network. Therefore, they have come up with guidelines on such distributed generators.

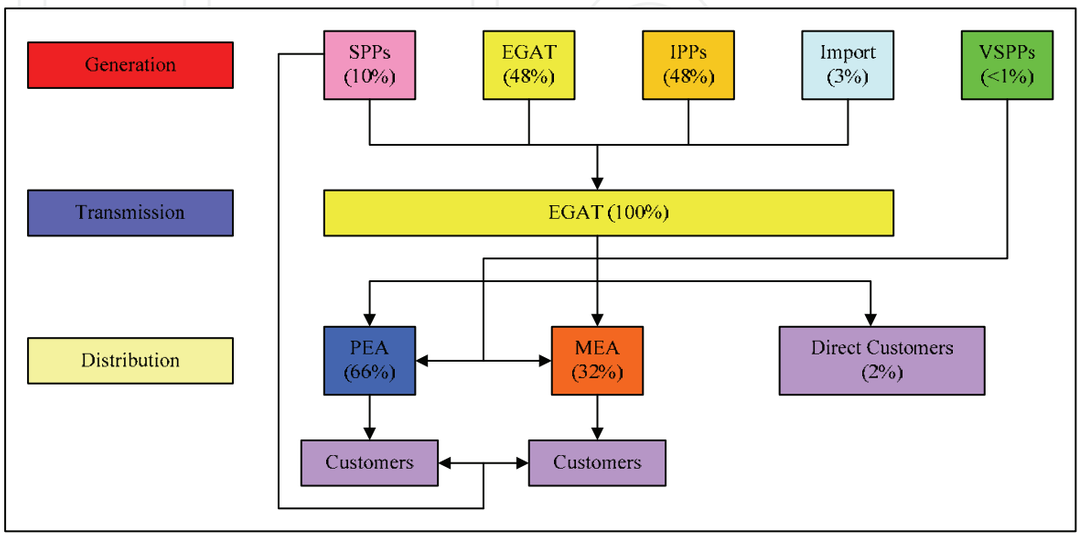

Fig 1. Structure of electricity industry of Thailand

The Power Development Plan – PDP of Thailand sets targets for electricity production from various sources [2]. The present one is PDP 2007. In 2008 148,197 million units were generated. Natural gas share is about 70% while renewable energy, excluding hydroelectric, is only 1.4%. From electricity forecasting of the national energy policy committee, Thailand has the peak power demand and energy demand approximately 44,281 MW and 288,920 million units in 2021. Natural gas would still the major source with 60% share and renewable energy, excluding hydroelectric, will increase to 2%. In order to promote electricity generation from renewable energy, SPPs and VSPPs will play a major role. To achieve this, economic and technology obstructions need to be removed. As a consequence, an extensive promotion program has been initiated through various mechanism such as the Renewable Portfolio Standard-RPS mandatory for the power producers, financial incentives, feed-in-tariff, adders, soft loans, and measures of the Board of Investment- BOI and tax reductions schemes [3].

The government establishes the RPS for power plants, mainly for EGAT. Consequently, new EGAT plants have to invest so that 5% of their electricity production comes from renewable energy sources such as solar cells, wind energy and waste to energy. However, power plants can either buy RPS credits from SPP operating on renewable energy. Furthermore, to motivate more electricity generation from renewable energy, adders for VSPPs are introduced, shown in Table 2.

Type of VSPPs	Capacity	New adder (Bath/kWh)	Duration(years)
Biomass	Capacity ≤ 1MW Capacity > 1MW	0.50 0.30	7 7
Biogas	Capacity ≤ 1MW Capacity > 1MW	0.50 0.30	7 7
Municipal waste	Digestion system Thermal system	2.50 3.50	7 7
Wind energy	Capacity ≤ 50 kW Capacity > 50 kW	4.50 3.50	10 10
Mini Hydro	Capacity 50-200 kW Capacity ≤ 50 kW	0.80 1.50	7 7
Solar PV		8.00	10

Table 2. Adders for VSPPs using renewable energy

1.2 Thai Utilities Guidelines on Distributed Generation

To assure the quality of power, stability, reliability and safety of operation, Thai utilities consider the effects of distributed generator-DG connecting to the power systems in many aspects and conditions. IPPs and SPPs are mainly involved with and, therefore, follow regulations of EGAT, the nature of guidelines are not covered in this paper. PEA and MEA will increasingly deal more with VSPPs and have come up with numbers of regulations on purchasing of power from VSPPs or DGs.

PEA and MEA regulations can be categorized into 3 groups, namely, first, the terms for connection of VSPPs to the electrical network, secondly, operation of grid-connected VSPPs, and thirdly, specifications of VSPPs connecting to the network [4] [5] [6][7].

On specifications of VSPPs, the followings are covered in guidelines : (i) Power capacity and voltage levels for connection, shown in Table 3, (ii) Voltage regulations, (iii) Short circuit levels, (iv) Power quality such as voltage fluctuations, frequencies, power factor and harmonics, (v) Protection systems, and (vi) Connection configurations of VSPPs.

On the connection configurations, MEA and PEA have identified types of VSPPs based on voltage levels, generator types, and power capacity. Examples are (i) synchronous generator rated not exceed to 1.25 MVA and rating of transformer not exceed 2.5 MVA for multi generators, (ii) single synchronous generator capacity more than 1 MW, (iii) multi synchronous generators with capacity more than 1 MW, (iv) single induction generator with capacity less than 5 MVA, (v) multi induction generators with capacity more than 5 MVA, (vi) single induction generator at low voltage, (vii) multi induction generators at low voltage, (viii) three-phase inverter at medium voltage, (ix) three- phase inverter at low voltage and (x) single phase inverter at low voltage.

Utility	Voltage Level	Normal Circumstances		Exceptional Circumstances		Short Circuit Level
		Min (kV)	Max (kV)	Min (kV)	Max (kV)	kA
MEA	115 kV	109.2	120.7	103.5	126.5	31.5-40
	69 kV	65.5	72.4	62.1	75.9	40

	33 kV	31.3	34.7	29.7	36.3	25
	22 kV	20.9	23.1	19.8	24.2	25
	380 V	342 V	418 V	342 V	418 V	10
	220 V	200 V	240 V	200 V	240 V	10
PEA	115 kV	106.4	117.6	96.0	123.0	31.5-40
	69 kV	63.6	70.4	57.3	72.5	40
	24 kV	21.8	23.6	21.6	24.0	25
	12 kV	10.9	11.8	10.8	12.0	25
	400 V	371 V	410 V	362 V	416 V	10
	230 V	214 V	237 V	209 V	240 V	10

Table 3. Maximum and minimum voltage level standard of MEA and PEA

The voltage levels of the networks at which DGs are connected are determined by the power capacity of DGs. For the DG with power capacity of more than 250 kW, the voltage level at medium level, i.e. 22-33 kV for PEA and 12-24 kV for MEA. For, DGs with capacity between 56 -250 kW, PEA and MEA will consider voltage level on a case by case basis. For DGs less than 56 kW, the voltage level is 380 V three-phase for PEA and 400V three-phase for MEA. For DGs less than 10 kW, connection is made at 220 V, single phase for PEA and 230 V single phase for MEA.

In relation to solar PV applications in Thailand, the past decade has seen shifts from PV used in the public market through government demonstration projects to the consumer market, with installations of numbers of PV VSPPs and domestic roof-top grid connected PV units gaining momentum. The latter approach has been adopted in Japan, Germany, Switzerland and, to a certain extent, in the U.S. to promote PV applications in a consumer market. It is envisaged that with the government incentive on adders on electricity generated from renewable energy, more households will be attracted to produce electricity from solar PV and wind energy. As domestic roof sizes are limited, PV roof-top grid-connected units will be of small capacity, less than 10 kW. It is this possible large expansion of market for small PV roof-top grid-connected units in Thailand, and eastern Asia, that draws our attention to the study of single phase PV grid-connected systems. Our focus will be on the anti-islanding protection study.

In connecting a single phase PV-based inverter to the power system, a basic configuration consists of PV generators, an inverter, a circuit breaker, and local loads, shown schematically in Fig 2 . Major features of the inverter used must comply with abovementioned regulations of utilities on

protections of undervoltage and overvoltage, phase and ground over-current, underfrequency and overfrequency, and anti-islanding protection. For other types of distributed generators, similar considerations hold.

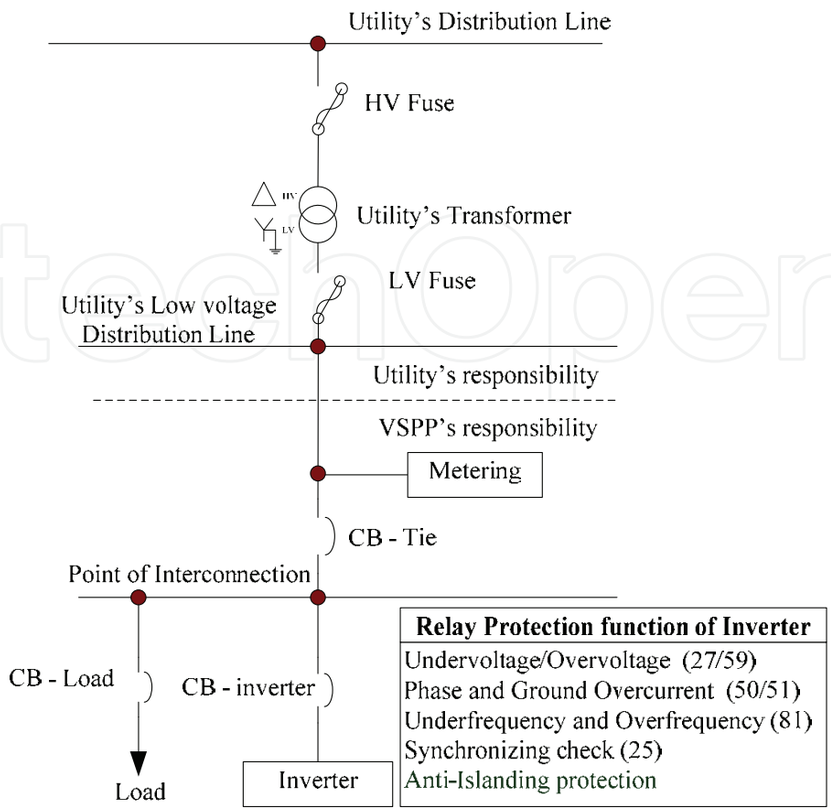

Fig. 2. Single phase inverter connection to the utility

Islanding Protection

The anti islanding function is one of requirement protection function of VSPP inverter based systems. Islanding phenomena is a condition in which the utility grid is disconnected from the distributed generation which still supplies to any section of local loads. Normally, the distributed generation is required to sense the absence of utility-controlled generation and cease energizing the grid. Otherwise, damages can occur to VSPP equipment if the generation in the islanding area, no longer under utility control, operates outside of normal voltage and frequency conditions. Besides, customer and utility equipment can be damaged if the main grid recloses into the island out of synchronization. Energized lines within the island present a shock hazard to unsuspecting utility line workers who think the lines have no electricity.

The anti-islanding protection must follow the regulations of PEA and MEA, requiring that after tripping an interconnection breaker or a fuse, the generator should separate from the system within 0.1 seconds. In addition, the inverter need to pass either

(i)the IEEE 929-2000 Recommended Practice for Utility Interface of Photovoltaic

Systems [8] and IEEE 1547.1-2005 Standard Conformance Test Procedures for Equipment Interconnecting Distributed Resources with Electric Power Systems [9], or

(ii) the IEC 62116 Test Procedure of Islanding Prevention Measures for Utility-Interconnected Photovoltaic Inverters [10] and the IEC 61727 Photovoltaic Systems-Characteristics of the Utility Interface [11].
In this study, the goal is to develop a mathematical model of a dc-ac full bridge switching converter voltage source with current control of a PV grid-connected system under islanding phenomena with the state-space averaging and piecewise technique. To simplify the mathematical models and equivalent circuits, some basic assumptions have been neglected such as the exclusion of parasitic elements effects (equivalent series inductance, ESL, of inductor-winding resistance and core loss or equivalent series resistance, ESR, of filter capacitors). The two proposed modelings, implemented by MATLAB/SIMULINK, are verified with the PSpice and experiments.

2. Modeling Single Phase PV-Based Inverter under Islanding Phenomena

2.1 Components of a PV-Grid Connected System under Study

In this study, the single phase photovoltaic system has been proposed. Fig 3 shows a block diagram of a voltage source inverter using a current control technique, applied for a PV grid-connected system in this study. This configuration is common for most available commercial units. The main components are a PV Panel, a DC-DC converter with an isolated transformer, a DC-AC converter, and a AC filter, a Phase Lock Loop (PLL), a Maximum Power Point Tracking (MPPT) unit, a PI controller and a Pulse Width Modulation (PWM) for switching scheme.

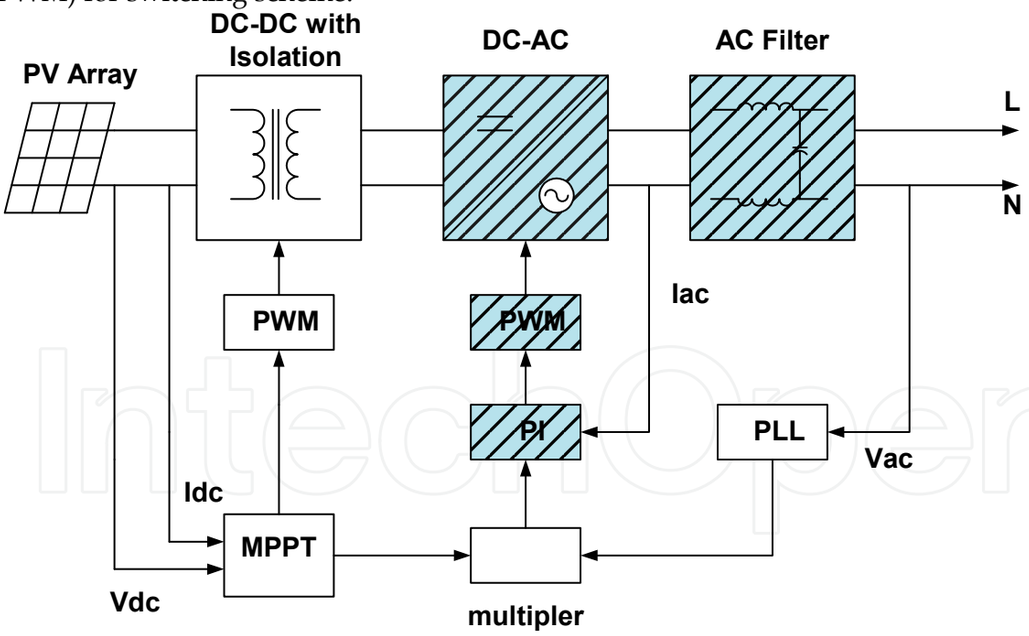

Fig. 3. Block diagram of a voltage source inverter with a current control.

PV Panel: generates direct current from sunlight. In this study, the PV panel is assumed to be a fixed DC voltage source neglecting the variation of sunlight.

DC-DC switching converter with isolated transformer [12][13]: There are several topologies for converting DC to DC voltage with desired values, for example, Push-Pull, Flyback, Forward, Half Bridge and Full Bridge. The choice for a specific application is often based on many considerations such as size, weight of switching converter, generation interference and economic evaluation. In this study, the full bridge configuration is designed for achieving the maximum power from PV application which is controlled with MPPT command. Also included is an isolated transformer commonly used to provide isolation between both sides of the DC input and output of AC systems. The main purpose of this is to eliminate the ground loops between circuitries.

DC-AC switching converter or inverter [14]: It is used to convert from DC to AC. Commonly, the inverter can be classified into two types (a) Voltage Source Inverter (VSI) if input voltage remains constant and (b) Current Source Inverter (CSI) if input current remains constant. The CSI is mostly used in large motor applications, whereas the VSI is adopted for and alone systems. The CSI is a dual of a VSI. In a VSI, the load current depends on the load impedance, whereas the load voltage in a CSI depends on the load impedance. The advantages of the CSI are (i) as the input dc current is controlled and limited, thus misfiring of switching device or short circuit would not be a serious problem (ii) peak current of the power device is limited (iii) the commutation circuit for thyristors are simple and (iv) it can handle reactive or regenerative load without freewheeling diodes. Both can use controlled turn-on and turn-off power electronics devices, for example, metal oxide semiconductor field effect transistor (MOSFET), bipolar junction transistors (BJT) and insulated gate bipolar transistors (IGBTs). Generally, the inverter uses pulse width modulation (PWM) control signals for generating the desired value.

A control technique for voltage source inverters consists of two types, a Voltage Control Inverter as shown in Fig.4 (a) and a Current Control Inverter as shown in Fig. 4 (b). The voltage control inverter is designed to control the angle between the inverter voltage and the grid voltage before synchronizing. In the case of the current control inverter, the output current from the inverter is controlled in phase with the grid voltage. The advantages of this are, first, peak current protection , secondly, extremely good dynamics, thirdly, control of instantaneous current waveform and high accuracy [15]. The disadvantages of current control are that it is costly due to current sensor device, and the difficulty to eliminate the noise signal from the sensed current especially with small current.

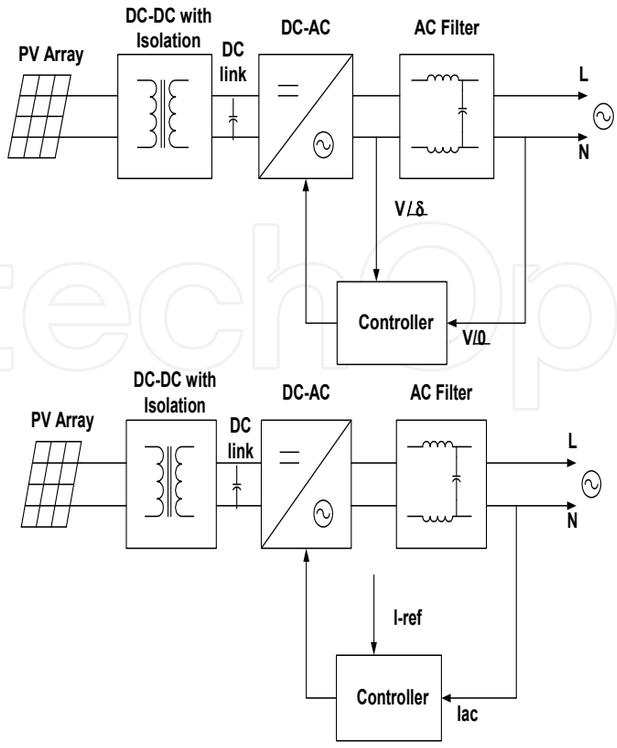

(a) Voltage Control Inverter (b) Current Control Inverter

Fig. 4. Control techniques for an inverter.

2.2 The Operation of Block Diagram of PV Grid Connected System with Current Control

The direct current and voltage from the PV panel are measured and formed as input for an MPPT block to generate the gate signal for a dc-dc converter in order to operate in maximum power generation mode. The current amplitude at maximum operation from MPPT block is multiplied with a unity sinusoidal waveform which is produced from Phase Locked Loop (PLL) block. Its result is designated as the current reference signal. At the output of a dc-ac converter stage, the actual current is sensed and compared with the current reference, then its error is compensated with PI controller which is called an error amplify stage. Finally, this output is compared with the saw-tooth signal to generate a PWM signal for gate drive of a dc-ac converter in a comparator stage.

In this study PV panel, a dc-dc converter with an isolated transformer, an MPPT and a PLL are neglected, therefore the shaded area in Fig.3 is focused and re-illustrated in Fig.5. The input source of a dc-ac switching converter is replaced with a constant DC source instead of a dc-dc switching converter. The switching converter configuration is a full bridge or H-bridge switching converter with a LC filter. The actual current inductor flowing through the filter is sensed for the feedback control loop. This current feedback is compared with constant current reference. The result of this is compensated with PI controller. A simple circuit of dc-ac switching converter is shown in Fig.6.

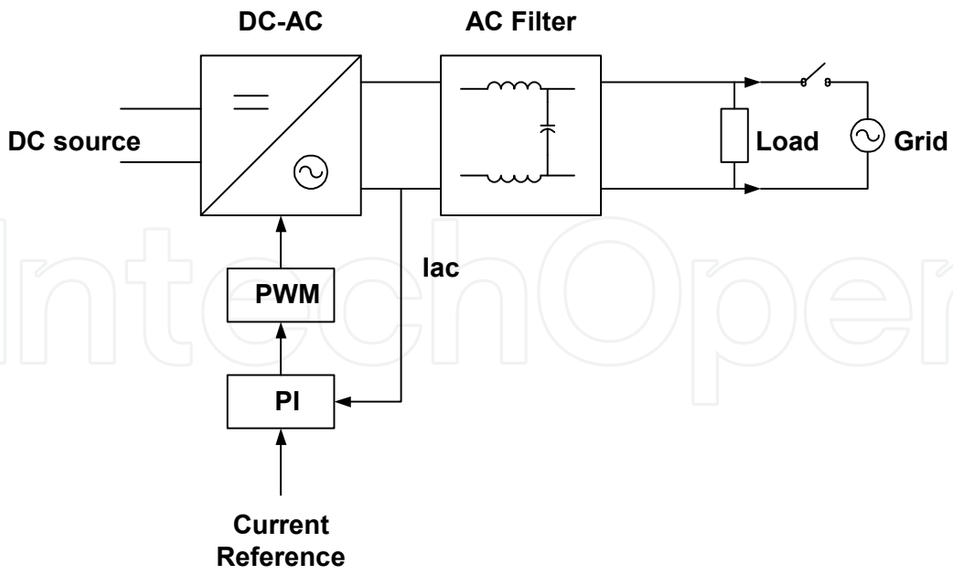

Fig. 5. Block diagram of dc-ac switching converter.

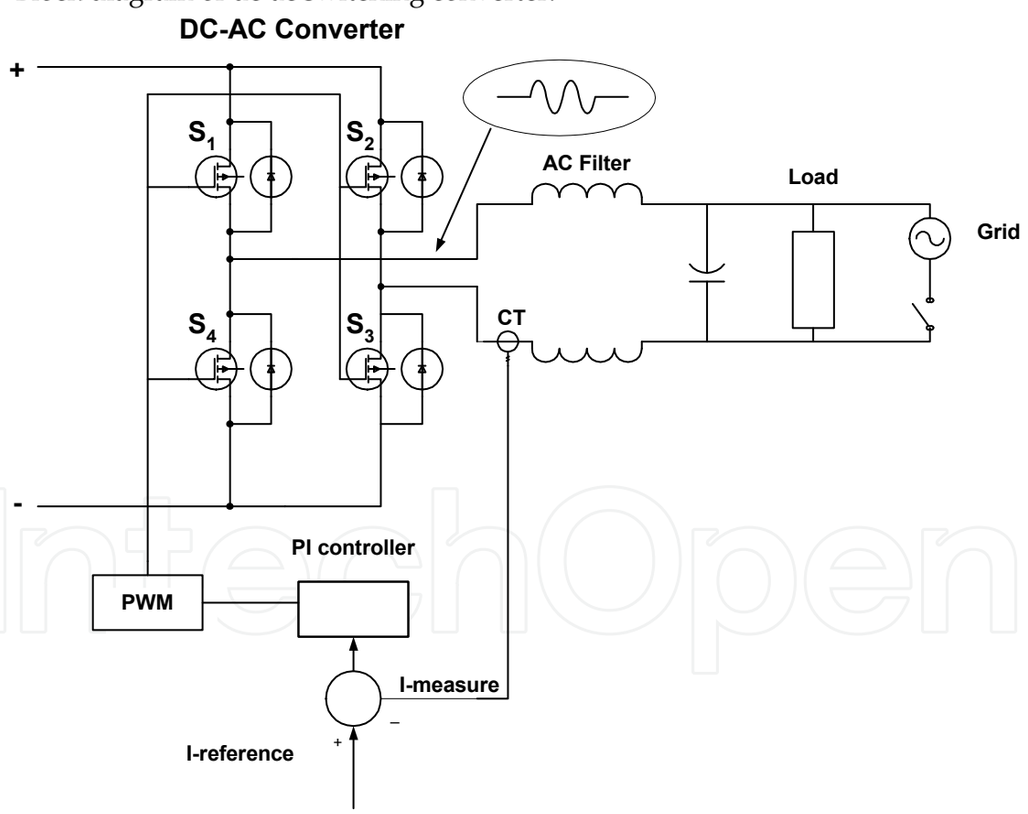

Fig. 6. A simple circuit of dc-ac full-bridge switching converter.

As shown in Fig.6, a pair of the switching converters S1- S3 and S2-S4 are operated alternately of a switching period with its duty cycle (d). The duty cycle (d) is the ratio of the

ON time (t_{on}) to the switching period (T), $d = \frac{t_{on}}{T} = t_{on} f_s$ and 1-d for OFF time as plotted in Fig 7. During one switching cycle, two circuits for the switch states of a dc-ac full bridge switching converter are shown in Fig. 8 (a) and (b) for S1-S3 ON state and S2-S4 ON state respectively. It is noted that the differences of both circuits are only the reversed polarity of input voltage (v_s).

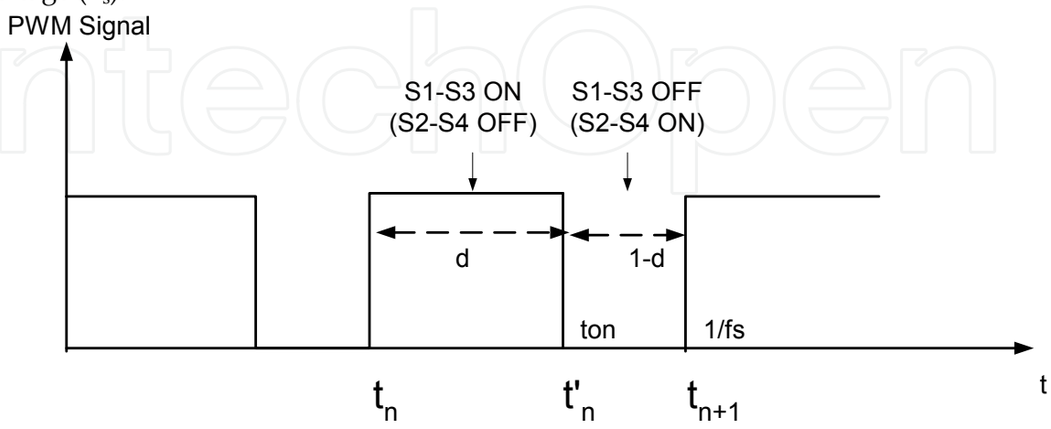

Fig. 7. PWM Signal for d and 1-d interval.

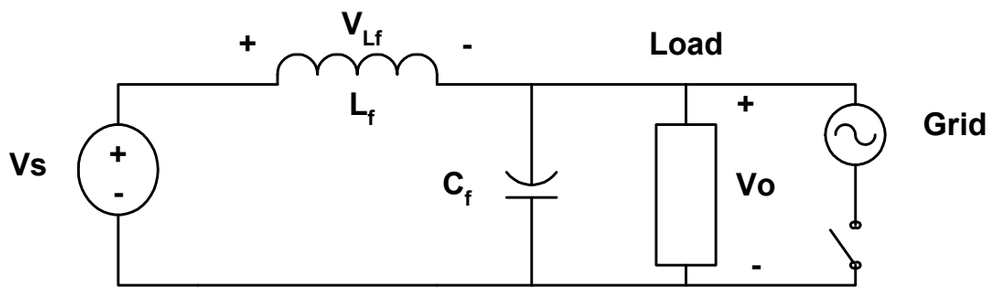

(a) S1-S3 ON state and S2-S4 OFF state.

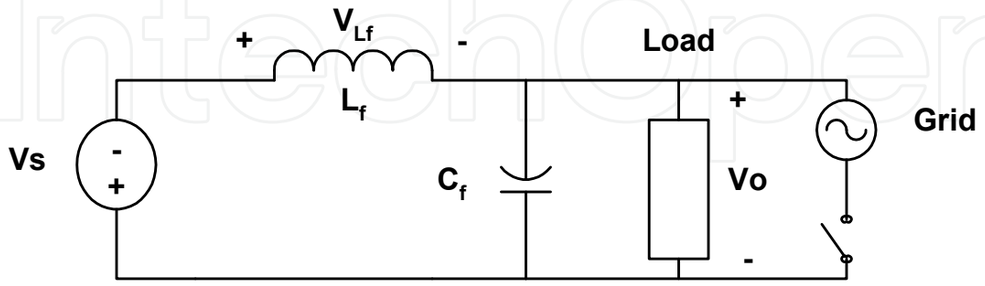

(b) S1-S3 OFF state and S2-S4 ON state.
Fig. 8. Circuit diagram during one switching cycle.

2.3 Voltage Conversion Ratio of a DC-AC Full-Bridge Switching Converter

To calculate the voltage conversion ratio, we use the fact that the averaging of inductor voltage $v_{L(avg)}$ per cycle must be zero in the steady stage. Therefore, we can identify two linear switched circuits modeling as follows:

- For S1-S3 ON state and S2-S4 OFF state, V_{Lf} is

$$V_{Lf} = V_S - V_O$$

The value of V_{Lf} with multiplied by D is given

$$(V_S - V_O)D \tag{1}$$

Where D = $t_{ON} f_s$

f_s = switching frequency

- For S1-S3 OFF state and S2-S4 ON state, V_{Lf} is

$$V_{Lf} = -(V_S - V_O)$$

The value of V_{Lf} with multiplied by (1-D) is equal to

$$-(V_S - V_O)(1 - D) \tag{2}$$

Combine Eq.(2.1) and Eq.(2.2) , we have the voltage conversion ratio as below;

$$(V_S - V_O)D - (V_S - V_O)(1 - D) = 0$$

$$\frac{V_O}{V_S} = 2D - 1 \tag{3}$$

Where D = duty cycle in steady state term

From the voltage conversion ratio in Eq.(3), it indicates that if the duty cycle (D) is set equal to 0.5, then the output voltage is zero value. In this study, the need for a dc-ac switching converter is to convert the DC signal into AC signal. That means that if we set the duty cycle (D) in terms of 0.5 + sinusoidal function, as a result, the output signal will be sinusoidal function across the x-axis. On the other hand, if we vary the DC term not to be 0.5 value, the output signal will be shifted above or below the x-axis with the DC term.

3. Analytical Methods

The switching converter can be represented by two basic methods, (i) a state-space averaging(in this study, non-linear behavior is focused, thus linearization is not performed) and (ii) a piecewise method [16] .

3.1 State-Space Averaging Modeling

Dynamic analysis is developed by using the state-space averaging technique developed by Middlebrook and Cuk. The main objective is to eliminate the time-varying parameters and it

is well suited for characterizing the switching converter in the low-frequency domain. Generally, it is performed in linearization terms for linear time-invariant models which can be analyzed in the standard frequency domain. However, this study aims to evaluate the islanding phenomena of a PV grid connected system which is nonlinear behavior, thus any linearization is not implemented.

Procedures for state-space averaging (no linearization) are as follows [12]:

identify a switched model over a switching cycle and draw a linear switched circuit for each state,

identify state variables and write state an equation in each state,

the d interval

$$\dot{\mathbf{x}} = \mathbf{A_1}\mathbf{x} + \mathbf{B_1}\mathbf{v} \tag{4}$$

the 1-d interval

$$\dot{\mathbf{x}} = \mathbf{A_2}\mathbf{x} + \mathbf{B_2}\mathbf{v} \tag{5}$$

Where $\mathbf{x}$ = state variable vector

$\mathbf{A}$ = state coefficient matrix

$\mathbf{v}$ = source vector

$\mathbf{B}$ = source coefficient matrix

perform state space averaging using the duty cycle as a weighting factor and combine state equations into a single averaged state equation as shown below:

$$\dot{\mathbf{x}} = \left[\overline{\mathbf{A}_1 d} + \overline{\mathbf{A_2}(1-d)}\right]\overline{x} + \left[\overline{\mathbf{B}_1 d} + \overline{\mathbf{B}_2}(1-d)\right]\overline{\mathbf{v}} \tag{6}$$

Where $\mathbf{x}$ = state variable vector

$\mathbf{A}$ = state coefficient matrix

$\mathbf{v}$ = source vector

$\mathbf{B}$ = source coefficient matrix

We note that any nonlinear continuous systems can be approximated as a linear system with a small neighborhood about its DC operating point. For example, duty cycle (d) comprises a steady state (DC) term designated by capital letter and a dynamic (AC) term by the "hat", as shown:

$$d = D + \hat{d}$$

To implement the state space averaging of a dc-ac full bridge switching converter with current control scheme, the converter can be divided into three sections, i.e. (a) power stage which comprises full-bridge switching configuration, a filter and resistive load R , (b) combination of resistive, inductive and capacitive loads, RLC and (c) a control stage which is a feedback current loop (an error amplify and comparator part), as shown in Fig.9.

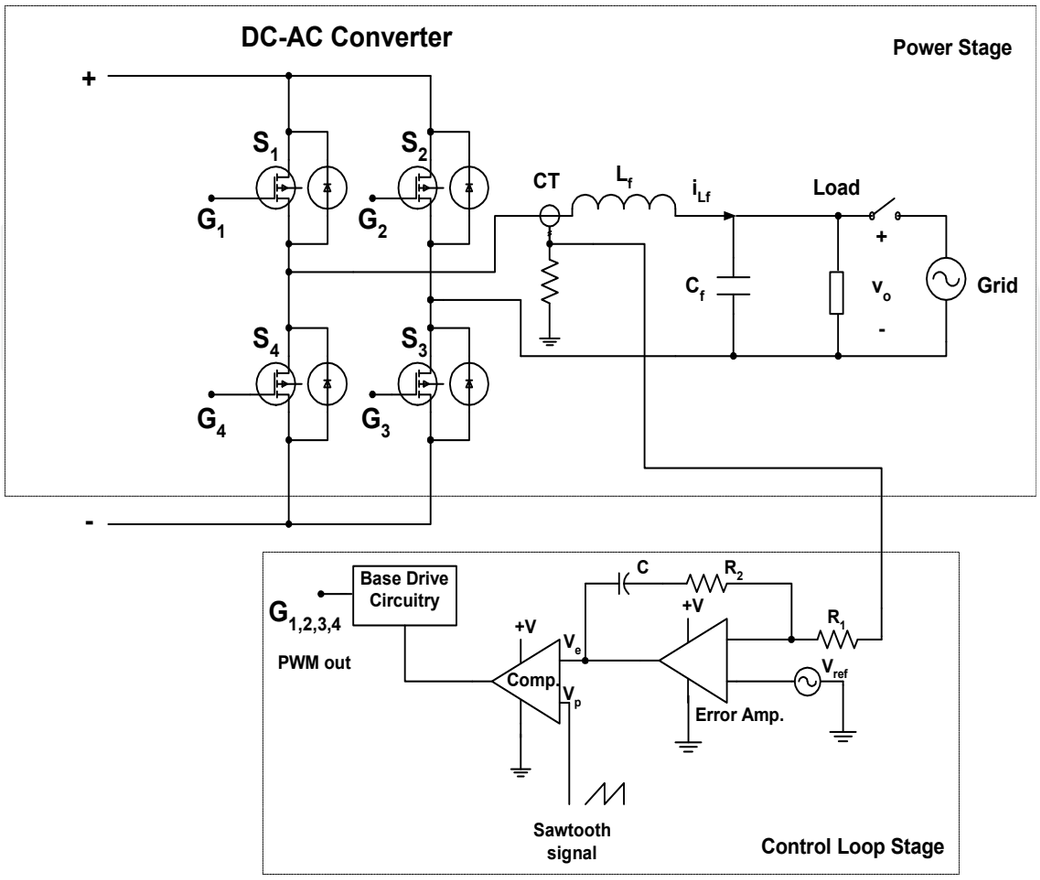

Fig. 9. Schematic diagram of a dc-ac full-bridge switching converter with a current control scheme for a resistive load (R).

Power stage for resistive load

The power stage is drawn in Fig.10 where the resistor is connected in parallel as load.

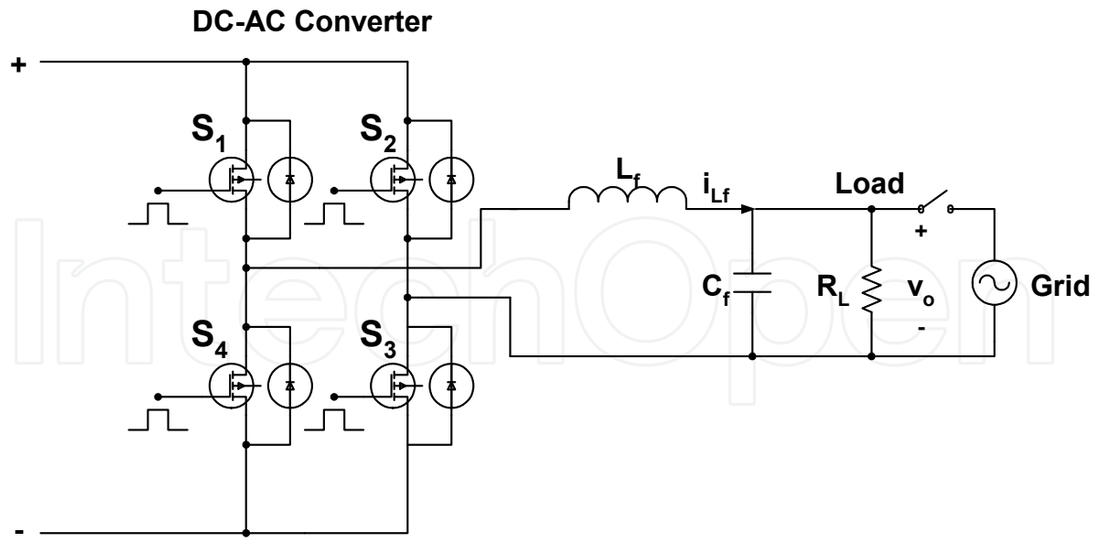

Fig. 10. Power stage for resistive load.

The equivalent circuit during S1and S3 ON, d interval (or S2 and S4 OFF) is illustrated in Fig. 11.

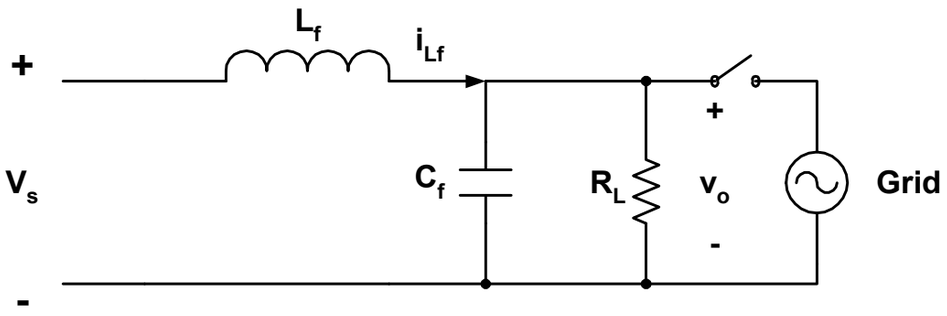

Fig. 11. Equivalent circuit during S1-S3 ON.

From Fig.11, the two state variables for this converter are considered as an inductor current flowing through the filter, i_{Lf} and a load voltage, v_o. Thus two state equations are

$$v_s - v_o = L_f \frac{di_{Lf}}{dt}$$

$$C_f \frac{dv_o}{dt} = i_{Lf} - \frac{v_o}{R_L}$$

Written in matrix, we have

$$\begin{bmatrix} \frac{di_{Lf}}{dt} \\ \frac{dv_o}{dt} \end{bmatrix} = \begin{bmatrix} 0 & \frac{-1}{L_f} \\ \frac{1}{C_f} & \frac{-1}{R_L C_f} \end{bmatrix} \begin{bmatrix} i_{Lf} \\ v_o \end{bmatrix} + \begin{bmatrix} \frac{1}{L_f} \\ 0 \end{bmatrix} \begin{bmatrix} v_s \end{bmatrix} \tag{7}$$

For 1-d interval, the equivalent circuit during S1and S3 OFF, 1-d interval (or S2 and S4 ON) is illustrated in Fig. 12.

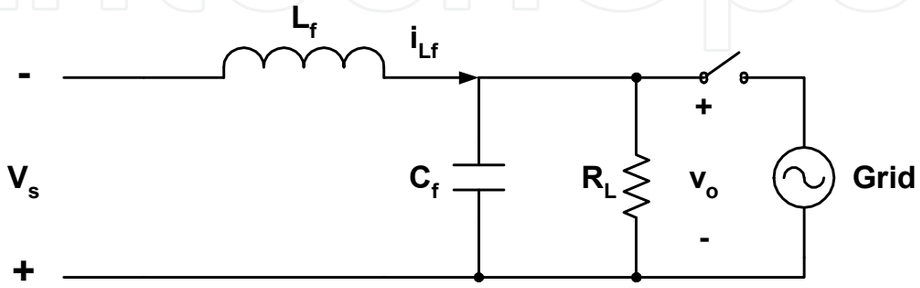

Fig. 12. Equivalent circuit during S1-S3 OFF.

Two linear state equations can be expressed by applying Kirchoff's voltage and current law, from Fig.12, as shown below:

$$v_s + v_o = -L_f \frac{di_{Lf}}{dt}$$

$$C_f \frac{dv_o}{dt} = i_{Lf} - \frac{v_o}{R_L}$$

Written in matrix, it becomes

$$\begin{bmatrix} \frac{di_{Lf}}{dt} \\ \frac{dv_o}{dt} \end{bmatrix} = \begin{bmatrix} 0 & \frac{-1}{L_f} \\ \frac{1}{C_f} & \frac{-1}{R_L C_f} \end{bmatrix} \begin{bmatrix} i_{Lf} \\ v_o \end{bmatrix} + \begin{bmatrix} \frac{-1}{L_f} \\ 0 \end{bmatrix} \begin{bmatrix} v_s \end{bmatrix} \tag{8}$$

From Eq.(7) and (8), we can calculate the state space averaged state coefficient matrix as expressed in Eq.(6). The result is

$$\mathbf{A} = \begin{bmatrix} 0 & \frac{-1}{L_f} \\ \frac{1}{C_f} & \frac{-1}{R_L C_f} \end{bmatrix} d + \begin{bmatrix} 0 & \frac{-1}{L_f} \\ \frac{1}{C_f} & \frac{-1}{R_L C_f} \end{bmatrix} (1-d)$$

$$\mathbf{A} = \begin{bmatrix} 0 & \dfrac{-1}{L_f} \\ \dfrac{1}{C_f} & \dfrac{-1}{R_L C_f} \end{bmatrix}$$

$$\mathbf{B} = \begin{bmatrix} \dfrac{1}{L_f} \\ 0 \end{bmatrix} d + \begin{bmatrix} \dfrac{-1}{L_f} \\ 0 \end{bmatrix} (1-d) = \begin{bmatrix} \dfrac{2d-1}{L_f} \\ 0 \end{bmatrix}$$

Therefore, we obtain the stage space average matrix as follows:

$$\begin{bmatrix} \dfrac{di_{Lf}}{dt} \\ \dfrac{dv_o}{dt} \end{bmatrix} = \begin{bmatrix} 0 & \dfrac{-1}{L_f} \\ \dfrac{1}{C_f} & \dfrac{-1}{R_L C_f} \end{bmatrix} \begin{bmatrix} i_{Lf} \\ v_o \end{bmatrix} + \begin{bmatrix} \dfrac{2d-1}{L_f} \\ 0 \end{bmatrix} \begin{bmatrix} v_s \end{bmatrix} \tag{9}$$

Power stage for RLC load

For the RLC load, the power stage which is connected with the combination of R, L and C in parallel as load is shown in Fig. 13. To simplify the state equation, the combination between the filter capacitor and the load capacitor is designated as C_{new} term. Therefore, an inductor current flowing through the filter i_{Lf}, an inductor current flowing through load i_{LL} and a load voltage v_o are chosen as state variables.

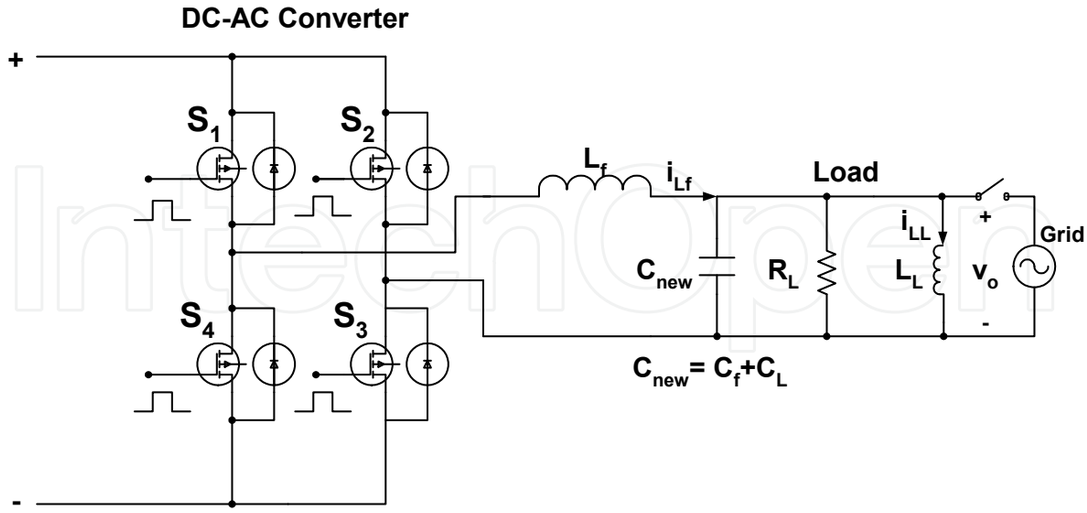

Fig. 13. Power stage for RLC load.

The equivalent circuit during S1and S3 ON, d interval (or S2 and S4 OFF) is illustrated in Fig. 14.

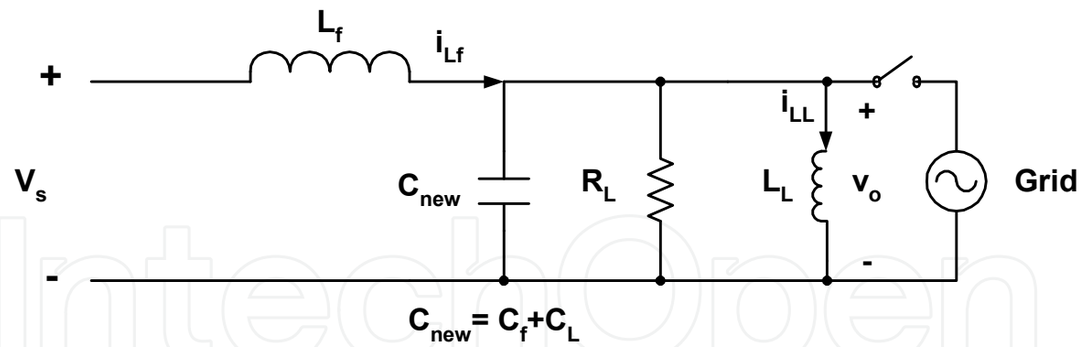

Fig. 14. Equivalent circuit during S1-S3 ON.

We can derive three linear state equations in d interval, from Fig.14, as follows:

$$v_s - v_o = L_f \frac{di_{L_f}}{dt}$$

$$v_o = L_L \frac{di_{LL}}{dt}$$

$$C_{new} \frac{dv_o}{dt} = i_{Lf} - i_{LL} - \frac{v_o}{R}$$

Written in a matrix form, it gives

$$\begin{bmatrix} \frac{di_{Lf}}{dt} \\ \frac{di_{LL}}{dt} \\ \frac{dv_o}{dt} \end{bmatrix} = \begin{bmatrix} 0 & 0 & \frac{-1}{L_f} \\ 0 & 0 & \frac{1}{L_L} \\ \frac{1}{C_{new}} & \frac{-1}{C_{new}} & \frac{-1}{R_L C_{new}} \end{bmatrix} \begin{bmatrix} i_{Lf} \\ i_{LL} \\ v_O \end{bmatrix} + \begin{bmatrix} \frac{1}{L_f} \\ 0 \\ 0 \end{bmatrix} \begin{bmatrix} v_s \end{bmatrix} \tag{10}$$

Also, for 1-d interval, the equivalent circuit can be drawn as in Fig. 15.

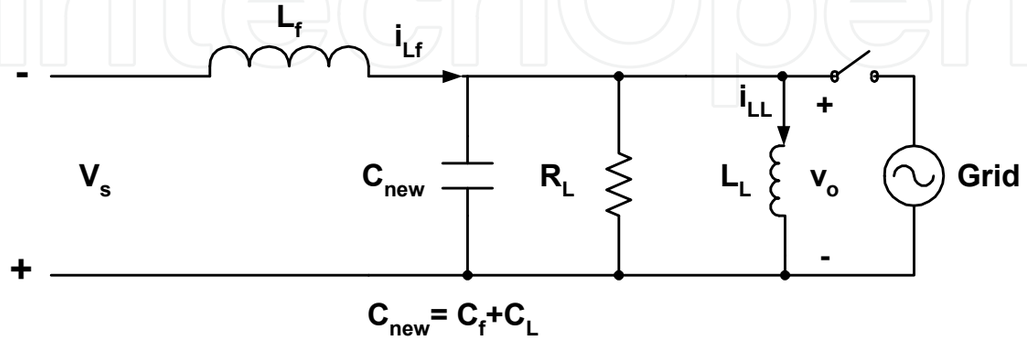

Fig. 15. Equivalent circuit during S1-S3 OFF.

From Fig. 15, the state equation is obtained by applying the Kirchoff's voltage and current law as follows:

$$-v_s - v_o = L_f \frac{di_{Lf}}{dt}$$

$$v_o = L_L \frac{di_{LL}}{dt}$$

$$C_{new} \frac{dv_o}{dt} = i_{Lf} - i_{LL} - \frac{v_o}{R_L}$$

Written in matrix form, we have

$$\begin{bmatrix} \frac{di_{Lf}}{dt} \\ \frac{di_{LL}}{dt} \\ \frac{dv_o}{dt} \end{bmatrix} = \begin{bmatrix} 0 & 0 & \frac{-1}{L_f} \\ 0 & 0 & \frac{1}{L_L} \\ \frac{1}{C_{new}} & \frac{-1}{C_{new}} & \frac{-1}{R_L C_{new}} \end{bmatrix} \begin{bmatrix} i_{Lf} \\ i_{LL} \\ v_o \end{bmatrix} + \begin{bmatrix} \frac{-1}{L_f} \\ 0 \\ 0 \end{bmatrix} \begin{bmatrix} v_s \end{bmatrix} \tag{11}$$

Similarly, from Eq.(10) and (11), we apply the averaging technique from Eq.(6), the nonlinear modeling can be represented as follows:

$$\begin{bmatrix} \frac{di_{Lf}}{dt} \\ \frac{di_{LL}}{dt} \\ \frac{dv_o}{dt} \end{bmatrix} = \begin{bmatrix} 0 & 0 & \frac{-1}{L_f} \\ 0 & 0 & \frac{1}{L_L} \\ \frac{1}{C_{new}} & \frac{-1}{C_{new}} & \frac{-1}{R_L C_{new}} \end{bmatrix} \begin{bmatrix} i_{Lf} \\ i_{LL} \\ v_o \end{bmatrix} + \begin{bmatrix} \frac{2d-1}{L_f} \\ 0 \\ 0 \end{bmatrix} \begin{bmatrix} v_s \end{bmatrix} \tag{12}$$

The stage space averaged equations from Eq.(9) and (12) for R and RLC load respectively are nonlinear equations because duty cycle (d) is a function of an inductor current flow through the filter, i_{Lf} .

Feedback current control stage

A feedback current control technique is implemented by controlling inductor currents flowing through filters corresponding to a reference current. As a result, the output current is in phase with grid voltages and produces a good power factor which controlled by a feedback current control loop stage consisting of sensing of inductor current flowing through the filter (i_{Lf}). The current is converted to a voltage form by multiplying with a resistor. Subsequently, this voltage is compared with a sinusoidal reference value. This stage is called "error amplification". Then the error amplification is compensated with the PI

controller. The result is designated as the error voltage (v_e). Finally, the error voltage is compared with the saw tooth signal to generate the PWM signal.

To model the dc-ac full-bridge switching converter and produce the output voltage in a sinusoidal waveform, we have to set up a duty cycle (d) with a variation in terms of a sinusoidal waveform around an average level of 0.5. This then provides [17]:

$$d(t) = 0.5 + m(\sin(\omega t)) \tag{13}$$

where m is a modulated duty cycle variation. The factor of 0.5 is determined from the relationship of voltage conversion ratio of the dc-ac full bridge switching converter, which is $v_o / v_s = 2d - 1$. Therefore, if v_s is dc source and d is represented from Eq.(13), then the output voltage (v_o) can produce the sinusoidal waveform across the x-axis. The term $m(\sin(\omega t))$ can be represented as $\frac{v_e(t)}{V_P}$. Thus, we can substitute it into Eq.(13) and obtain

$$d(t) = 0.5 + v_e(t)/V_p \tag{14}$$

As shown in Fig. 16, we can calculate $v_e(t)$ with a basic Op-amp circuit calculation as shown below:

The current flowing through R_1 is

$$i_{R1} = \frac{v_{iLf-} v_{ref}}{R_1}$$

The current flowing through R_2 is

$$v_{ref} - v_e = i_{R2} R_2 + v_C$$

Applying the Kirrchoff's current law, that is $i_{R1} = i_{R2}$ and $v_C = \frac{1}{C}\int i_{R2} dt$, thus we have

$$v_e(t) = v_{ref}(1 + \frac{R_2}{R_1}) - v_{i\,Lf}(\frac{R_2}{R_1}) - \frac{1}{C\,R_1}\int v_{i\,Lf} dt + \frac{1}{C\,R_1}\int v_{ref} dt \tag{15}$$

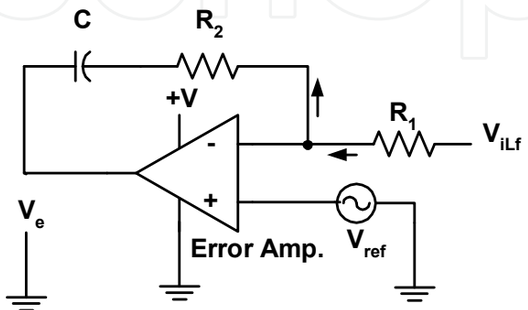

Fig. 16. Error amplification circuit with a PI controller.

We obtain the duty cycle (d) in a time domain by substituting $v_e(t)$ from Eq.(15) into Eq.(14). We construct a nonlinear differential equation model by using Eq.(9), (12) and (14) for power stages of R loads, RLC loads, and duty cycle (d) from a feedback current control stage, respectively.

The solution of a nonlinear differential equation can easily be handled by MATLAB computation as well as passive detection method as shown in Fig. 17.

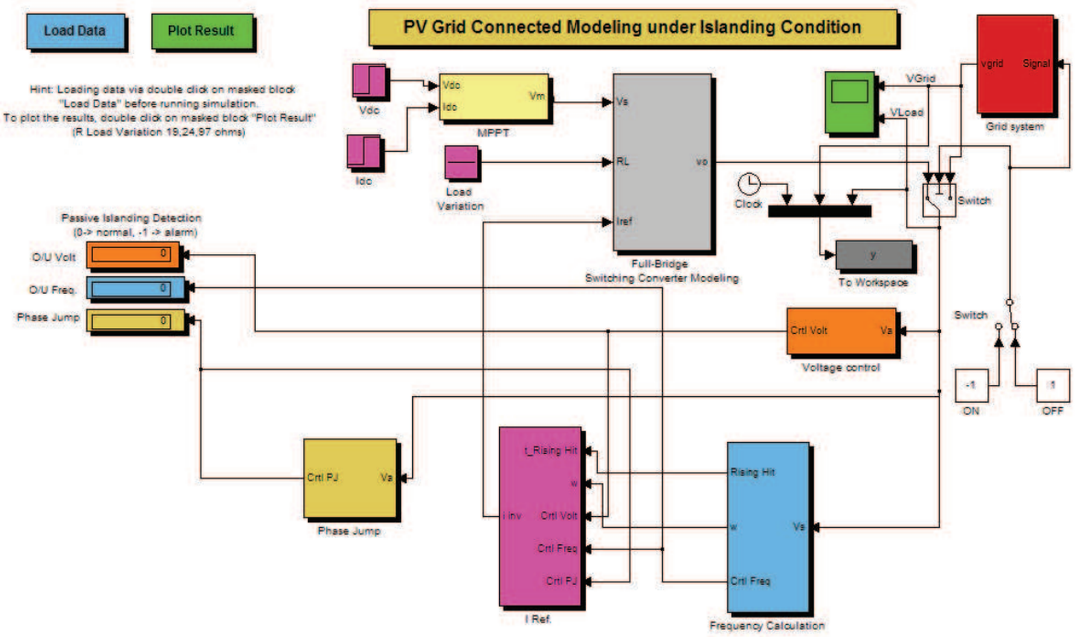

Fig. 17. Proposed modeling of PV grid connected on MATLAB/SIMULINK.

3. 2 Piecewise Technique Modeling

The basic idea of the piecewise technique is the point by point conversion of a continuous time signal (A/D) with a sampling period (T) as illustrated in Fig. 18

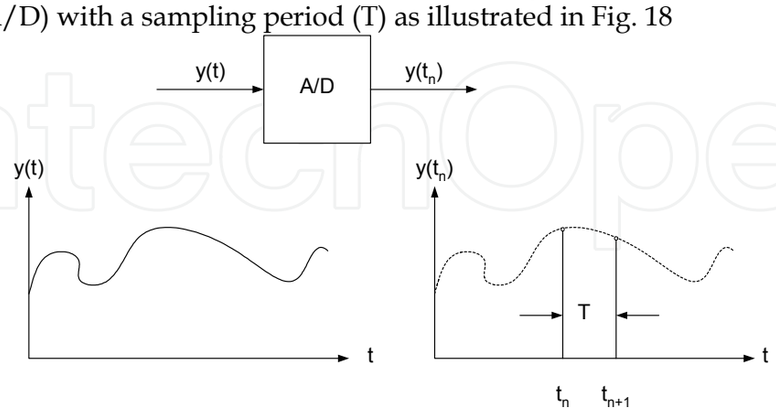

Fig. 18. Basic conversions from continuous time signal into piecewise signal.

During one switching cycle of a switching converter, the operation consists of each piece at a particular interval of time and then they repeat themselves periodically. Thus, it is

straightforward to model such kind of operation by splitting the system into several sub-system topologies corresponding to time sub-intervals. For the solution at a particular time, this consists of taking an initial value at specific sub-circuit and solving it. Then, we continue to solve the next sub-circuit with the previous solution as the initial value. The main concept of piecewise technique model involves the substitution of the solution of previous sub-interval as the initial condition of the sub-interval under consideration The flow chart is shown in Fig.19.

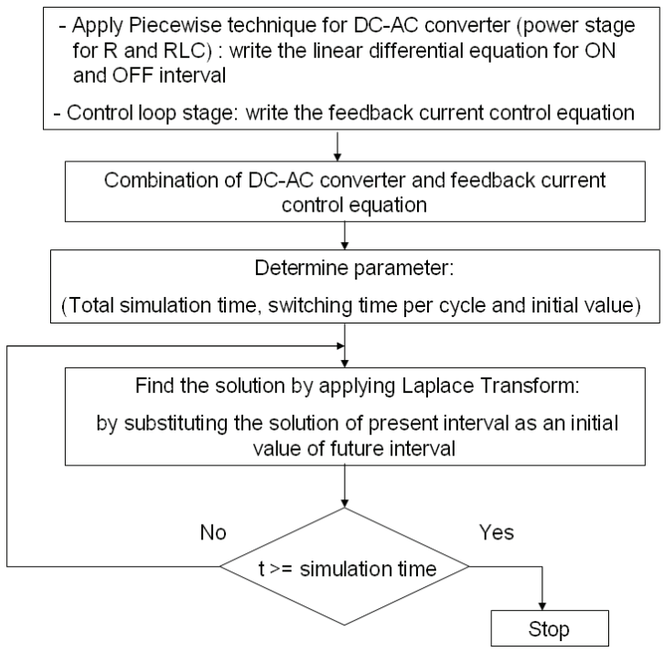

Fig. 19. Flow chart for a proposed model.

In doing so, firstly we write down the state equations which describe the individual switched circuit of a multi-topological circuit. The inverter operates in continuous conduction mode. Thus, two switched circuits can be identified, one for the 'switch-on' interval (S1 and S3 ON) and the other to 'switch-off' interval (S1 and S3 OFF). Two state equations can be derived by applying the Kirchoff's voltage and current laws. We solve the state-space equation of the switch-on and switch- off intervals from Eq.(4) and (5) by using the Laplace transformation which is obtained in s-domain as shown below:

$$\mathbf{x}(s) = \left[s\mathbf{I} - \mathbf{A}_{\mathbf{(1)\,or(\,2)}}\right]^{-1}\left[x(t_{initial}) + \mathbf{B}_{\mathbf{(1)\,or\,(2)}}V_s(s)\right] \tag{16}$$

Following this, the partial fraction technique is applied for splitting up a ratio of large polynomials into a sum of ratios of small polynomials, for example:

$$Y(s) = \frac{s+1}{(s+2)^2} = \frac{A}{s+2} + \frac{B}{(s+2)^2}$$

Then, this result with the partial fraction can be easily taken using an inverse Laplace transformation into the time domain with standard inverse Laplace forms. Finally, the piecewise method is implemented in each interval as explained above.
To analyze the behavior of a DC-AC full-bridge switching converter PV grid-connected system under islanding phenomena, similarly to the state-space averaging method, we have to split this circuit into three sections, for power stage; (a) a resistive load, R; (b) a combination of resistive, inductive and capacitive load, RLC and control stage and (c) feedback current control.

Power stage for resistive load
The power stage is illustrated Fig. 10 where the resistor is connected in parallel as a load. The equivalent circuit during S1 and S3 ON, d interval or $t_n \le t < t_n^{'}$ (or S2 and S4 OFF) is illustrated in Fig. 11 and the state equation in Eq.(7). For the 1-d interval, the equivalent circuit during S1 and S3 OFF is illustrated in Fig. 12 and Eq.(8).
The state-space equation of the switch-on and-off interval is solved by using the Laplace transformation, then the partial fraction technique is applied , and taking the inverse Laplace transform. The solution is

$$i_{Lf}(t) = K_{1R-on} + \frac{K_{3R-on} - K_{2R-on}\sigma}{\omega} e^{-\sigma(t-t_n)} \sin\omega(t-t_n) + K_{2R-on} e^{-\sigma(t-t_n)} \cos\omega(t-t_n) \tag{17}$$

$$v_o(t) = K_{4R-on} + \frac{K_{6R-on} - K_{5R-on}\sigma}{\omega} e^{-\sigma(t-t_n)} \sin\omega(t-t_n) + K_{5R-on} e^{-\sigma(t-t_n)} \cos\omega(t-t_n) \tag{18}$$

where $\sigma = \frac{1}{2C_f R_L}$, $\omega = \sqrt{\frac{1}{L_f C_f} - \sigma^2}$

$$K_{1R-on} = \frac{v_s}{R_L}, \qquad K_{2R-on} = i_{Lf}(t_n) - \frac{v_s}{R_L}$$

$$K_{3R-on} = \frac{i_{Lf}(t_n)}{R_L C_f} - \frac{v_o(t_n)}{L_f} + \frac{v_s}{R_L}\left(\frac{R_L}{L_f} - 2\sigma\right), \quad K_{4R-on} = v_s$$

$$K_{5R-on} = v_o(t_n) - v_s, \qquad K_{6R-on} = \frac{i_{Lf}(t_n)}{C_f} - 2v_s\sigma$$

Following this, inserting $t = t_n^{'}$ and $t_n^{'} - t_n = dT = t_{on}$ in switch-on interval into Eq. (17) and (18), we can obtain the value of i_{Lf} and v_o at the end of switch-on interval as expressed:

$$i_{Lf}(t_n^{'}) = K_{1R-on} + \frac{K_{3R-on} - K_{2R-on}\sigma}{\omega} e^{-\sigma(dT)} \sin\omega(dT) + K_{2R-on} e^{-\sigma(dT)} \cos\omega(dT) \tag{19}$$

$$v_o(t_n^{'}) = K_{4R-on} + \frac{K_{6R-on} - K_{5R-on}\sigma}{\omega} e^{-\sigma(dT)} \sin\omega(dT) + K_{5R-on} e^{-\sigma(dT)} \cos\omega(dT) \tag{20}$$

Since K-values are a function of $\mathbf{x}(t_n)$, we can write the general form of the difference equation in the switch-on interval, which involves the value of $\mathbf{x}(t_n)$ as initial value and *d*. The equation is

$$\mathbf{x}(t_n^{'}) = \mathbf{f}(\mathbf{x}(t_n), d) \tag{21}$$

For switch (S1,S3)-off interval $t_n^{'} \le t < t_{n+1}$, in this interval, $\mathbf{x}(t_n^{'})$ value, which is the solution value of the previous interval or switch-on interval, is determined as the initial value. Similar to the switch-on interval, the expression of the solution from Eq. (8) can be obtained:

$$i_{Lf}(t) = K_{1R-off} + \frac{K_{3R-off} - K_{2R-off}\sigma}{\omega} e^{-\sigma(t-t_n^{'})} \sin\omega(t-t_n^{'}) + K_{2R-off} e^{-\sigma(t-t_n^{'})} \cos\omega(t-t_n^{'}) \tag{22}$$

$$v_o(t) = K_{4R-off} + \frac{K_{6R-off} - K_{5R-off}\sigma}{\omega} e^{-\sigma(t-t_n^{'})} \sin\omega(t-t_n^{'}) + K_{5R-off} e^{-\sigma(t-t_n^{'})} \cos\omega(t-t_n^{'}) \tag{23}$$

where

$$K_{1R-off} = -\frac{v_s}{R_L}, \qquad K_{2R-off} = i_{Lf}(t_n^{'}) - \frac{v_s}{R_L}$$

$$K_{3R-off} = \frac{i_{Lf}(t_n^{'})}{R_L C_f} - \frac{v_o(t_n^{'})}{L_f} + \frac{v_s}{R_L}(2\sigma - \frac{R_L}{L_f}), \quad K_{4R-off} = -v_s$$

$$K_{5R-off} = v_o(t_n^{'}) + v_s, \qquad K_{6R-off} = \frac{i_{Lf}(t_n^{'})}{C_f} + 2v_s\sigma$$

In this interval, we substitute $t = t_{n+1}$ then, $t_{n+1} - t_n^{'} = (1-d)T = t_{off}$ into Eq. (22) and (23), then we can obtain the value of i_{lf} and v_o at the end of switch-off interval as

$$i_{Lf}(t_{n+1}) = K_{1R-off} + \frac{K_{3R-off} - K_{2R-off}\sigma}{\omega} e^{-\sigma(1-d)T} \sin\omega(1-d)T + K_{2R-off} e^{-\sigma(1-d)T} \cos\omega(1-d)T \tag{24}$$

$$v_o(t_{n+1}) = K_{4R-off} + \frac{K_{6R-off} - K_{5R-off}\sigma}{\omega} e^{-\sigma(1-d)T} \sin\omega(1-d)T + K_{5R-off} e^{-\sigma(1-d)T} \cos\omega(1-d)T \tag{25}$$

From Eq. (24) and (25), the general form of the difference equation in the switch-off interval can be expressed

$$\mathbf{x}(t_{n+1}) = \mathbf{f}(\mathbf{x}(t_n^{'}), d) \tag{26}$$

To determine the general form of difference equation in one switching period, the $\mathbf{x}(t_n^{'})$ value of switch-on interval and the $\mathbf{x}(t_{n+1})$ value of switch-off interval are combined by substituting $\mathbf{x}(t_n^{'})$ in Eq. (21) with Eq. (26). Thus, the general form of difference equation is

$$\mathbf{x}(t_{n+1}) = \mathbf{f}(\mathbf{x}(t_n), d) \tag{27}$$

3.3 Power stage for RLC loads

For RLC loads, the combination of R, L and C are connected in parallel as load, as in Fig.12. The state equations of d and 1-d interval are expressed in Eq.(10) and (11) respectively: Similar to R load, Eq. (10) and (11) are solved by taking the Laplace transformation and re-arranging it to a partial fraction, then taking the inverse Laplace. The solution of S1and S3 ON, d interval is

$$i_{Lf}(t_n^{'}) = K_{1RLC-on} + K_{2RLC-on}dT + \frac{K_{4RLC-on} - K_{3RLC-on}\sigma_1}{\omega_{RLC}} e^{-\sigma_1(dT)} \sin \omega_{RLC}(dT) + K_{3RLC-on} e^{-\sigma_1(dT)} \cos \omega_{RLC}(dT) \quad (28)$$

$$i_{LL}(t_n^{'}) = K_{5RLC-on} + K_{6RLC-on}dT + \frac{K_{8RLC-on} - K_{7RLC-on}\sigma_1}{\omega_{RLC}} e^{-\sigma_1(dT)} \sin \omega_{RLC}(dT) + K_{7RLC-on} e^{-\sigma_1(dT)} \cos \omega_{RLC}(dT) \quad (29)$$

$$v_o(t_n^{'}) = K_{9RLC-on} + \frac{K_{11RLC-on} - K_{10RLC-on}\sigma_1}{\omega_{RLC}} e^{-\sigma_1(dT)} \sin \omega(dT) + K_{10RLC-on} e^{-\sigma_1(dT)} \cos \omega_{RLC}(dT) \quad (30)$$

Where $\sigma_1 = \frac{1}{2C_{new}R_L}$, $\omega_{RLC} = \sqrt{\frac{L_L + L_f}{L_L L_f C_{new}} - {\sigma_1}^2}$

$$K_{1RLC-on} = (\frac{L_f L_L C_{new}}{L_f + L_L})(\frac{i_{Lf}(t_n)}{C_{new}L_L} + \frac{v_s}{R_L C_{new} L_f} + \frac{i_{LL}(t_n)}{C_{new}L_f} - \frac{K_{2RLC-on}}{R_L C_{new}})$$

$$K_{2RLC-on} = \frac{v_s}{L_f + L_L}$$

$$K_{3RLC-on} = i_{Lf}(t_n) - K_{1RLC-on}$$

$$K_{4RLC-on} = \frac{i_{Lf}(t_n)}{R_L C_{new}} + \frac{v_s}{L_f} - \frac{v_o(t_n)}{L_f} - \frac{K_{1RLC-on}}{R_L C_{new}} + K_{2RLC-on}$$

$$K_{5RLC-on} = (\frac{L_f L_L C_{new}}{L_f + L_L})(\frac{i_{Lf}(t_n)}{C_{new}L_L} + \frac{i_{LL}(t_n)}{C_{new}L_f} - \frac{K_{6RLC-on}}{R_L C_{new}})$$

$$K_{6RLC-on} = \frac{v_s}{L_f + L_L}$$

$$K_{7RLC-on} = i_{LL}(t_n) - K_{5RLC-on}$$

$$K_{8RLC-on} = \frac{i_{LL}(t_n)}{R_L C_{new}} + \frac{v_o(t_n)}{L_L} - \frac{K_{5RLC-on}}{R_L C_{new}} - K_{6RLC-on}$$

$$K_{9RLC-on} = \frac{v_s L_L}{L_f + L_L}$$

$$K_{10RLC-on} = v_o(t_n) - K_{9RLC-on}$$

$$K_{11RLC-on} = \frac{i_{LL}(t_n) - i_{Lf}(t_n)}{C_{new}} - \frac{K_{9RLC-on}}{R_L C_{new}}$$

From Eq. (28), (29) and (30) we can write the general form of the difference equation in the switch-on interval as follows:

$$\mathbf{x}(t_n^{'}) = \mathbf{f}(\mathbf{x}(t_n), d) \tag{31}$$

The solution of S1and S3 OFF, 1-*d* interval is

$$i_{Lf}(t_{n+1}) = K_{1RLC-off} + K_{2RLC-off}(1-d)T + \frac{K_{4RLC-off} - K_{3RLC-off}\sigma_1}{\omega_{RLC}} e^{-\sigma_1(1-d)T} \sin\omega_{RLC}(1-d)T + K_{3RLC-off} e^{-\sigma_1(1-d)T} \cos\omega_{RLC}(1-d)T \tag{32}$$

$$i_{LL}(t_{n+1}) = K_{5RLC-off} + K_{6RLC-off}(1-d)T + \frac{K_{8RLC-off} - K_{7RLC-off}\sigma_1}{\omega_{RLC}} e^{-\sigma_1(1-d)T} \sin\omega_{RLC}(1-d)T + K_{7RLC-off} e^{-\sigma_1(1-d)T} \cos\omega_{RLC}(1-d)T \tag{33}$$

$$v_o(t_{n+1}) = K_{9RLC-off} + \frac{K_{11RLC-off} - K_{10RLC-off}\sigma_1}{\omega_{RLC}} e^{-\sigma_1(1-d)T} \sin\omega_{RLC}(1-d)T + K_{10RLC-off} e^{-\sigma_1(1-d)T} \cos\omega_{RLC}(1-d)T \tag{34}$$

where

$$K_{1RLC-off} = \left(\frac{L_f L_L C_{new}}{L_f + L_L}\right)\left(\frac{i_{Lf}(t^{'}_n)}{C_{new}L_L} - \frac{v_s}{R_L C_{new} L_f} + \frac{i_{LL}(t^{'}_n)}{C_{new}L_f} - \frac{K_{2RLC-off}}{R_L C_{new}}\right)$$

$$K_{2RLC-off} = \frac{-v_s}{L_f + L_L}$$

$$K_{3RLC-off} = i_{Lf}(t^{'}_n) - K_{1RLC-off}$$

$$K_{4RLC-off} = \frac{i_{Lf}(t^{'}_n)}{R_L C_{new}} - \frac{v_s}{L_f} - \frac{v_o(t^{'}_n)}{L_f} - \frac{K_{1RLC-off}}{R_L C_{new}} + K_{2RLC-off}$$

$$K_{5RLC-off} = \left(\frac{L_f L_L C_{new}}{L_f + L_L}\right)\left(\frac{i_{Lf}(t^{'}_n)}{C_{new}L_L} + \frac{i_{LL}(t^{'}_n)}{C_{new}L_f} - \frac{K_{6RLC-off}}{R_L C_{new}}\right)$$

$$K_{6RLC-off} = \frac{-v_s}{L_f + L_L}$$

$$K_{7RLC-off} = i_{LL}(t^{'}_n) - K_{5RLC-off}$$

$$K_{8RLC-off} = \frac{i_{LL}(t^{'}_n)}{R_L C_{new}} + \frac{v_o(t^{'}_n)}{L_L} - \frac{K_{5RLC-off}}{R_L C_{new}} - K_{6RLC-off}$$

$$K_{9RLC-off} = \frac{-v_s L_L}{L_f + L_L}$$

$$K_{10RLC-off} = v_o(t'_n) - K_{9RLC-off}$$

$$K_{11RLC-off} = \frac{i_{LL}(t'_n) - i_{Lf}(t'_n)}{C_{new}} - \frac{K_{9RLC-off}}{R_L C_{new}}$$

From Eq. (32), (33) and (34) we can write the general form of the difference equation in the switch-off interval. It is

$$\mathbf{x}(t_{n+1}) = \mathbf{f}(\mathbf{x}(t'_n), d) \tag{35}$$

To obtain the general form of difference equation in one switching period, the $\mathbf{x}(t'_n)$ value of switch-on interval and the $\mathbf{x}(t_{n+1})$ value of switch-off interval are combined by substituting $\mathbf{x}(t'_n)$ into Eq. (31) with Eq. (35). Thus, the general form of difference equation is

$$\mathbf{x}(t_{n+1}) = \mathbf{f}(\mathbf{x}(t_n), d) \tag{36}$$

Now, we can construct a completed differential equation model by using Eq.(27),(36) and (14) for the power stage with R load, RLC load and the duty cycle (d) from a feedback current control stage respectively.

The solution for such a model can readily be handled using simple numerical iteration methods with sampling time by using embedded MATLAB function on MATLAB/SIMULINK with the passive islanding method and PLL block [18] as shown in Fig. 20.

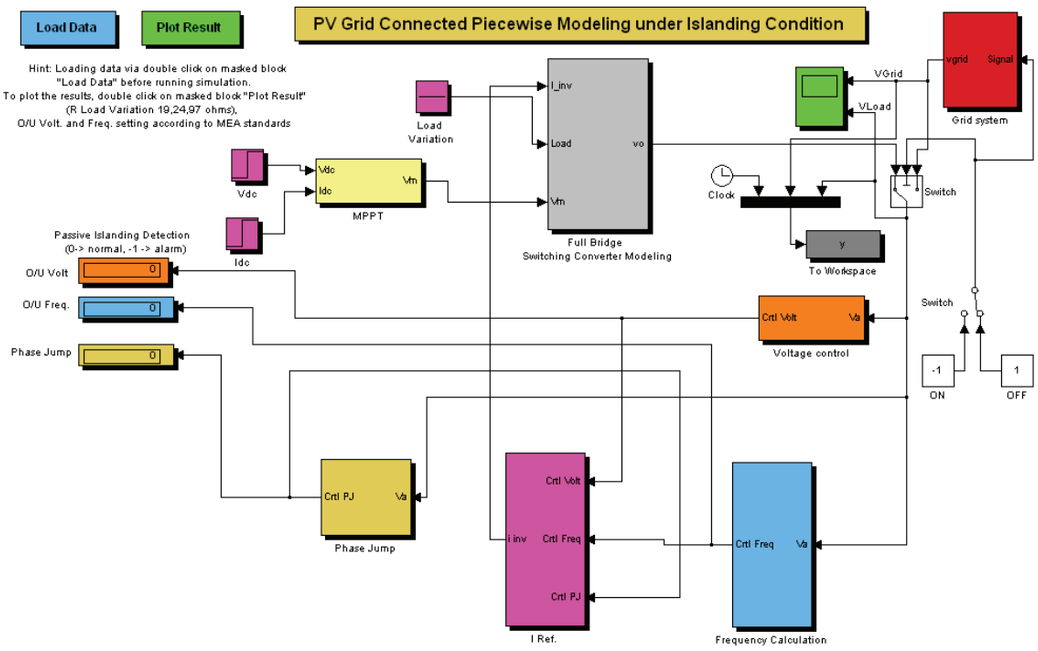

Fig. 20. The proposed model on MATLAB/SIMULINK.

4. Experimental Set Up and Results

The islanding test circuit, as shown in Fig.20, is set up to validate the two proposed modelings under islanding condition. The grid voltage reference and load voltage waveform are recorded from the oscilloscope for analysis with various load types. The various load types and adjustment of the ratios of the real load to an inverter output are undertaken and connected in parallel with the inverter. The input source of the inverter is a fixed a dc supply instead of a PV array to avoid the uncertainty of sunlight intensity. A 2 kW inverter purchased locally is used in this experiment.

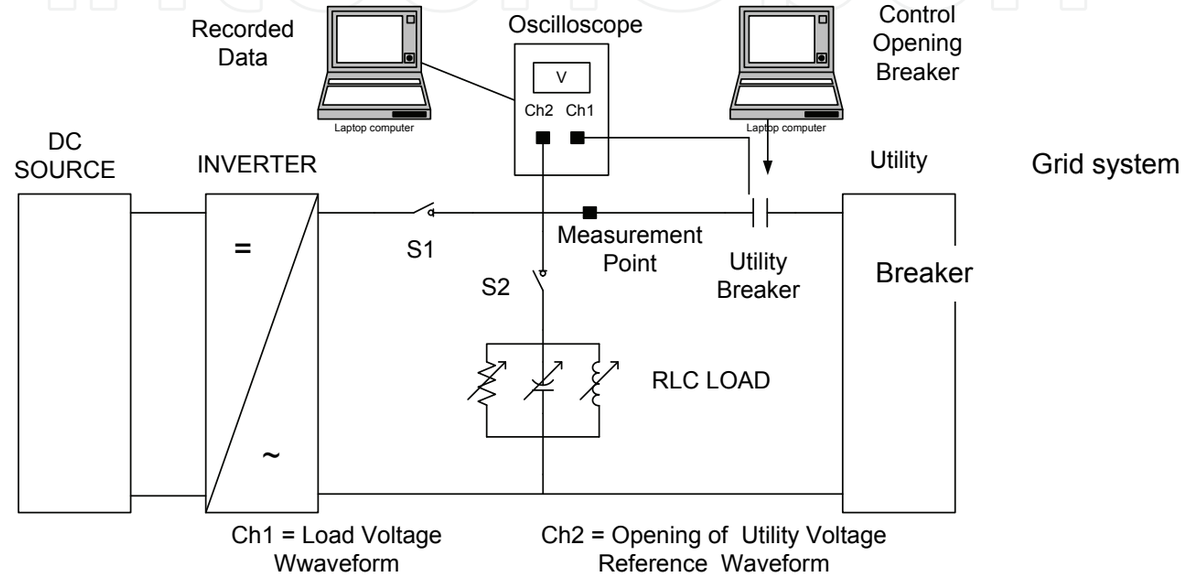

Fig. 20. Islanding test circuit.

Components used in the study

L_f = 2mH

C_f = 6.8 μ F

R_L = 19, 24 and 97 ohms (125%, 100% and 25% of the inverter output)

C_L = 2.66 μ F

L_L = 3.55H

R_1, R_2 = 10k, 25k ohms

C = 470 μ F

V_p = 6V

f_s = 10kHz

v_S = 450Vdc

I_{ref} = 1.5Aac

R_{ref} = 1.0 ohm
r = 0.1

Initially, the grid system is connected to the inverter, and then removed intentionally in order to form an islanding condition. For the experiment, the inverter is automatically stopped with its own islanding detection. The islanding detection of the proposed model and PSpice have been implemented with the passive method such as O/U voltage and O/U frequency as well as phase jump methods by sensing the output voltage. To avoid the malfunction of islanding detection, the inverter will be delayed 2-3 cycles before shutdown. The results between experiments, PSpice and the proposed model for various resistive load types and RLC load are compared under 3 different resistive loads: 125%, 100% and 25% and RLC. The results are plotted in Fig.21,22,23 and 24. The grid voltage is plotted as reference in the upper trace, superimposing values from measurement, the PSpice Program, the state space method and the piecewise method and the lower trace is the load voltage with similar superposition.

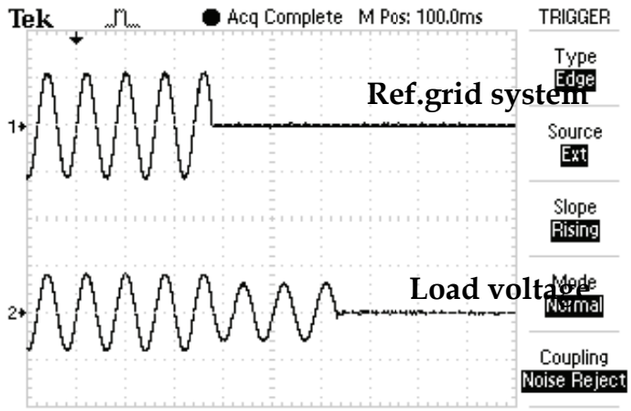

(a) Experiment result

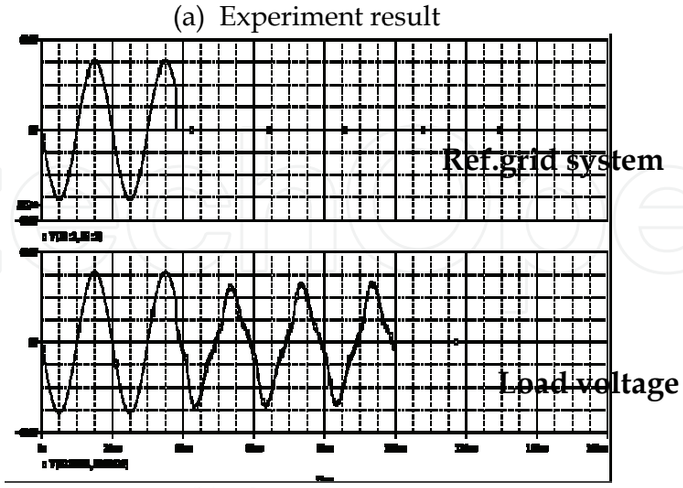

(b) PSpice Program

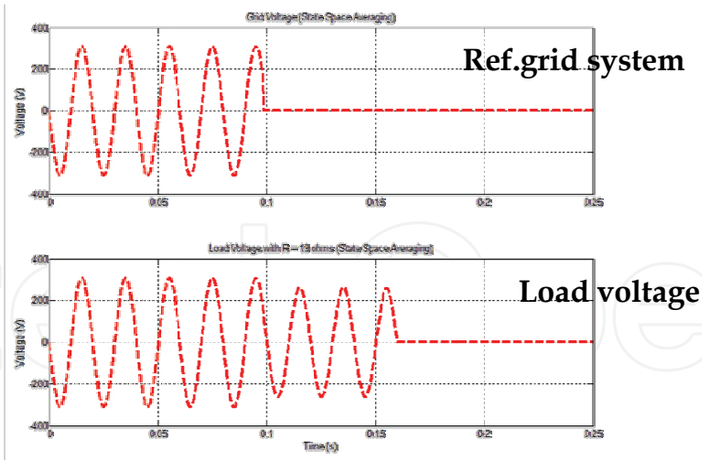

(c) State space averaging modeling

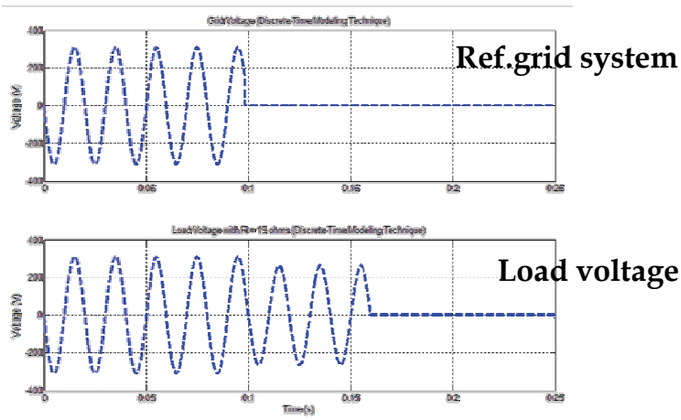

(d) Piecewise techniques modeling

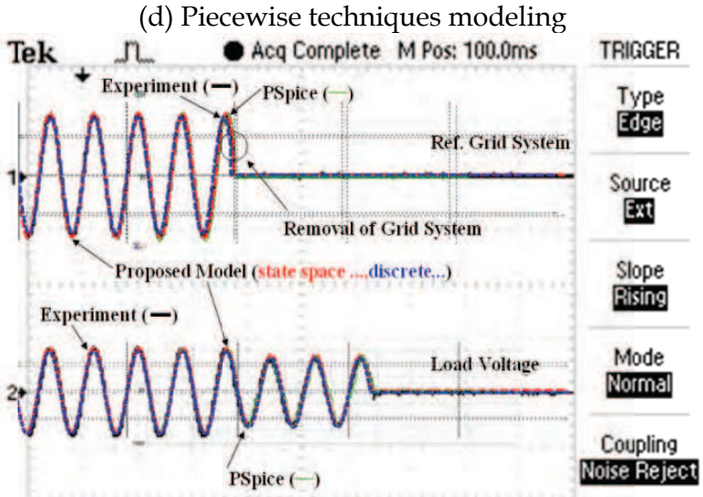

(e) Comparison of grid voltage (top) and load voltage (bottom) from experiment results, the PSpice Program, the state space method and the piecewise method

Fig. 21. Comparison of results for resistive load of 125% inverter output.

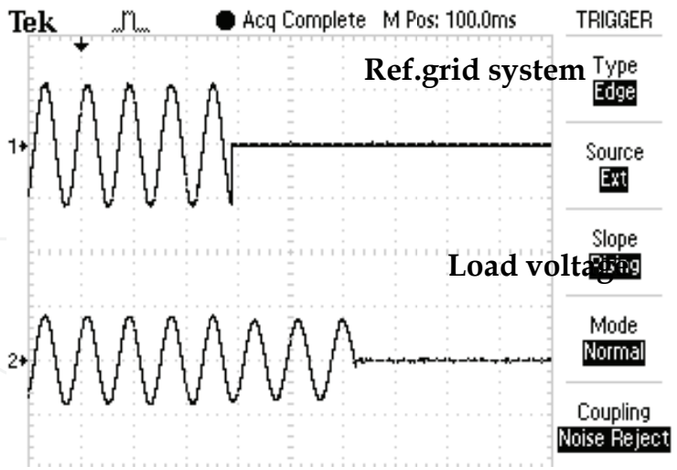

(a) Experiment result

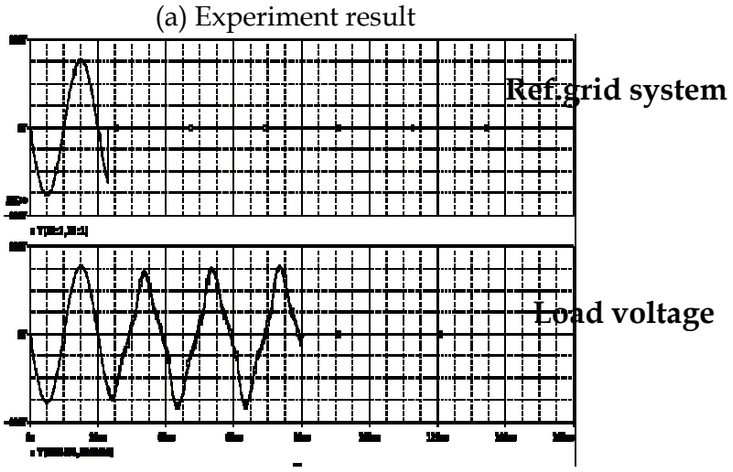

(b) PSpice Program

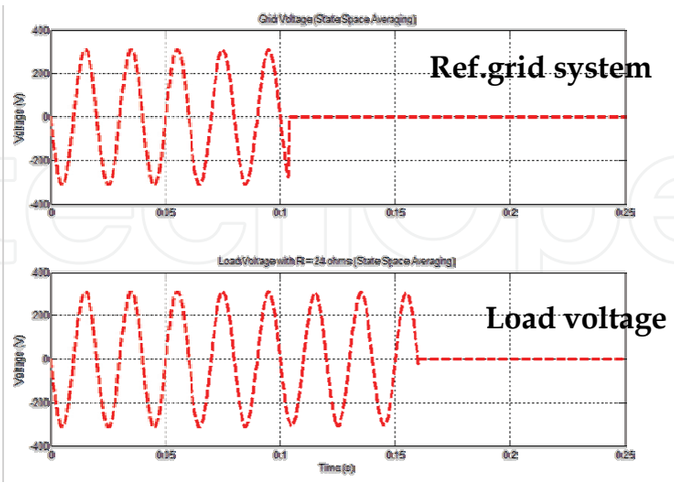

(c) State space averaging modeling

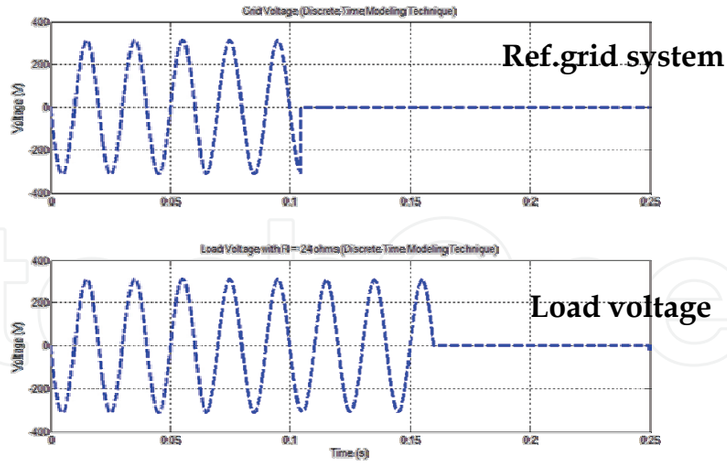

(d) Piecewise techniques modeling

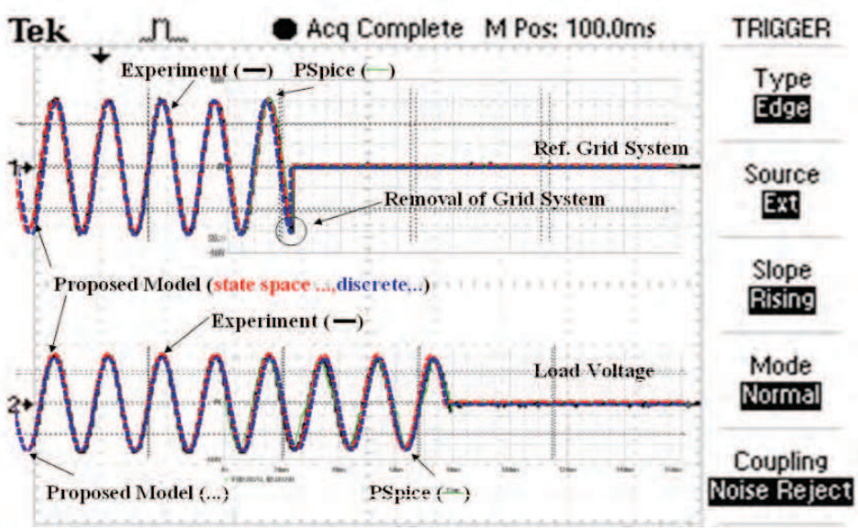

(e) Comparison of grid voltage (top) and load voltage (bottom) from experiment results, the PSpice Program, the state space method and the piecewise method

Fig. 22. Comparison of results for resistive load of 100% inverter output.

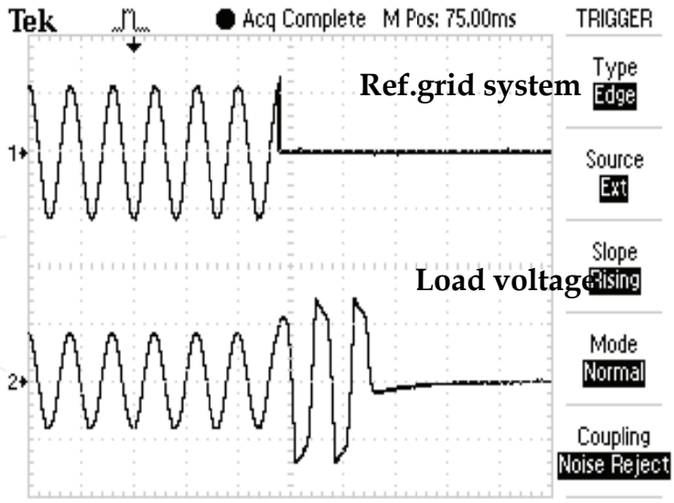

(a) Experiment result

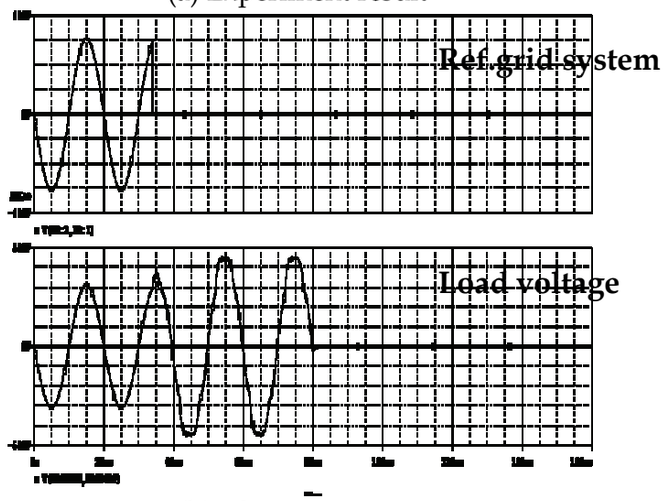

(b) PSpice Program

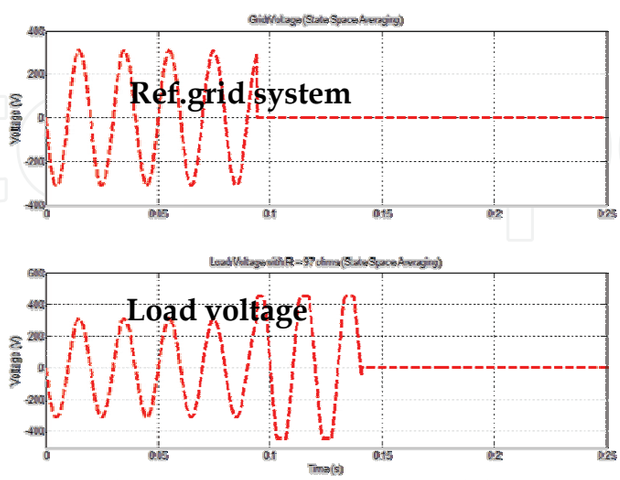

(c) State space averaging modeling

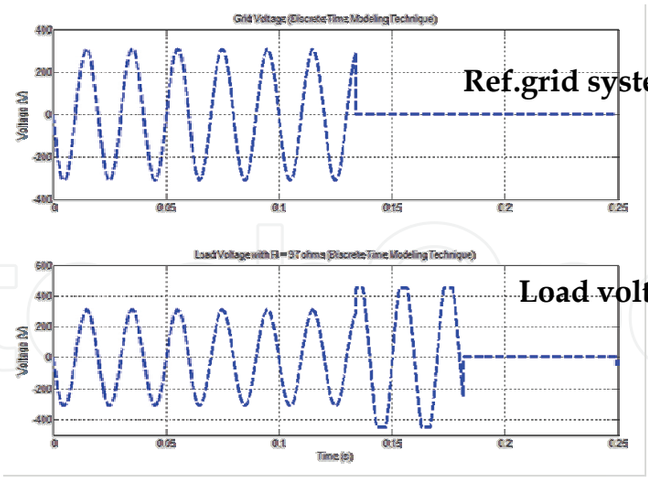

(d) Piecewise techniques modeling

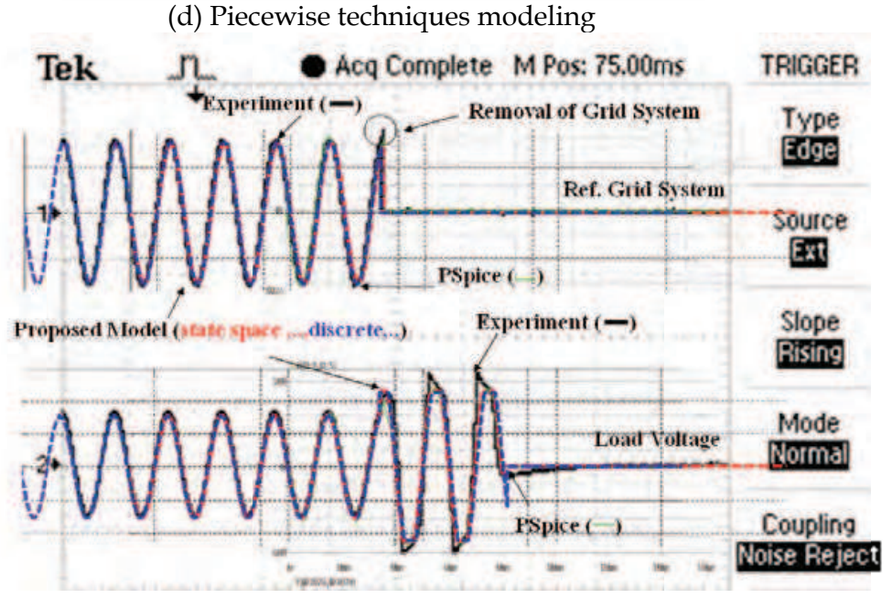

(e) Comparison of grid voltage (top) and load voltage (bottom) from experiment results, the PSpice Program, the state space method and the piecewise method

Fig. 23. Comparison of results for resistive load of 25% inverter output.

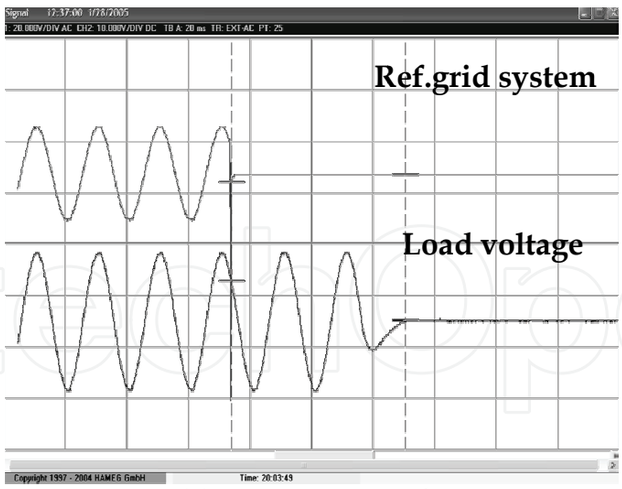

(a) Experiment result

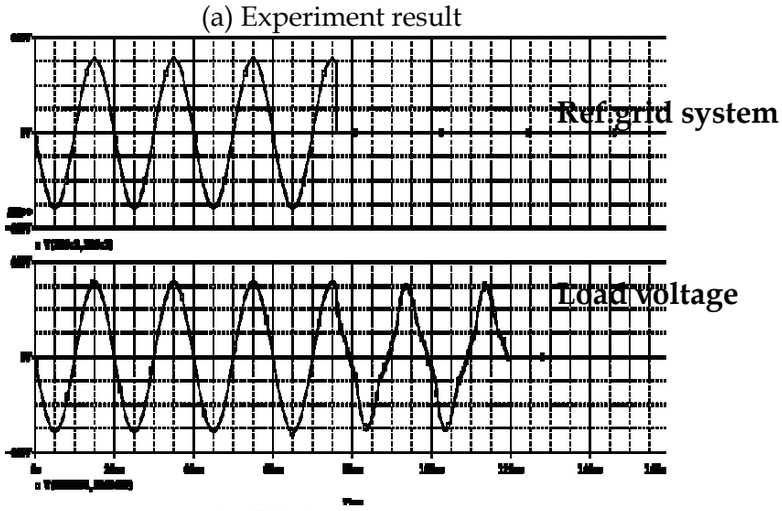

(b) PSpice Program

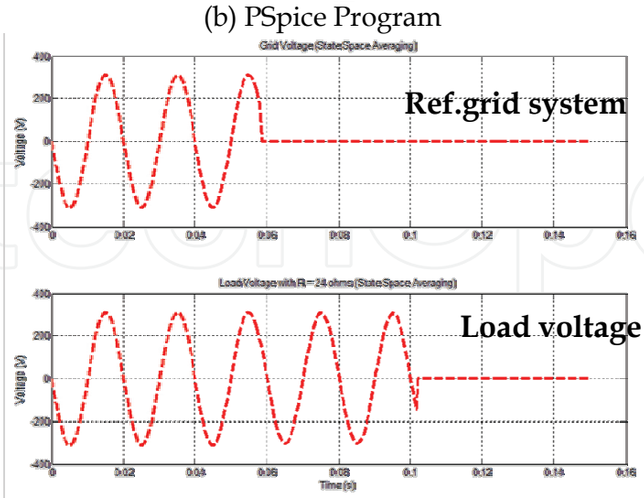

(c) State space averaging modeling

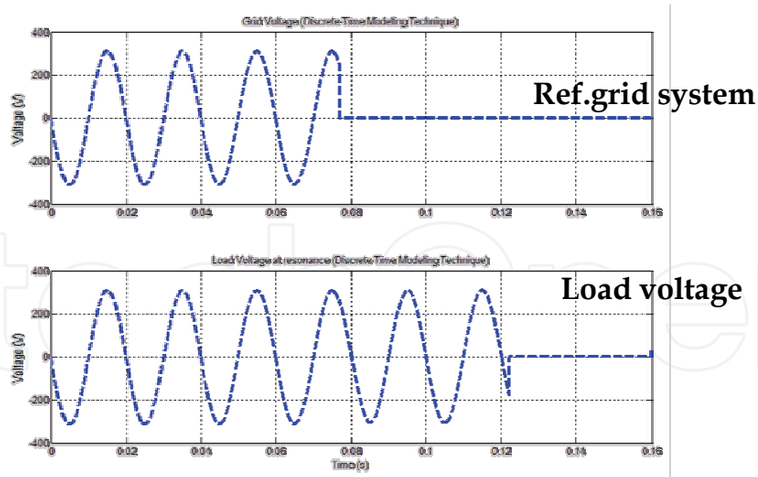

(d) Piecewise technique modeling

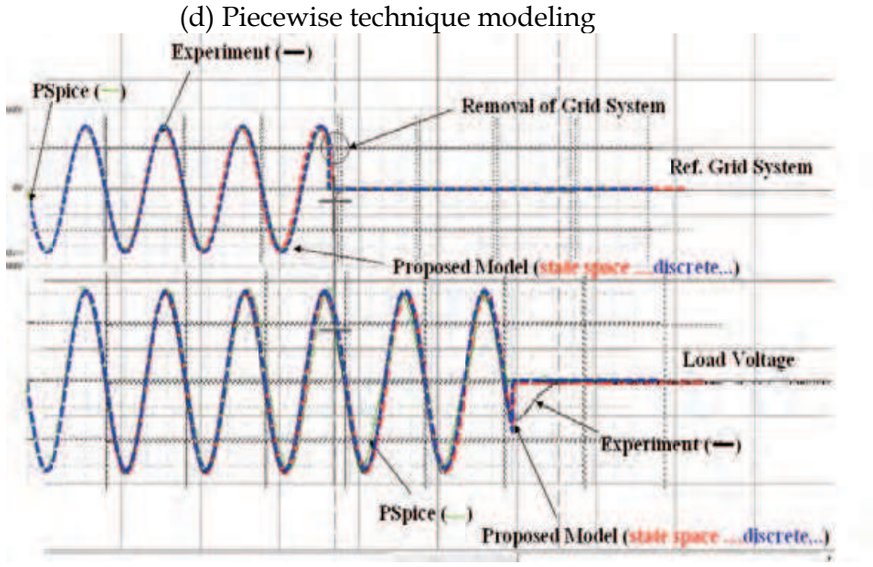

(e) Comparison of grid voltage (top) and load voltage (bottom) from experiment results, the PSpice Program, the state space method and the piecewise method

Fig. 24. Comparison of results for an RLC load resonance case.

Comparisons of the results obtained from the two proposed models are close to the experiment and the PSpice results. When the grid is tripped, the islanding detection from the proposed model can cease to energize within 2-3 cycles or 40-60 ms which pass the criteria of utility's standard as similar to experiment and the PSpice simulation. However, there are some differences due to parasitic element effects which were not considered in the proposed modeling. In case of a resistive load of 125% and 100%, the inverter behaves as current source. The load voltage waveform can give a perfect sinusoidal signal, as shown in Fig.21,22 (a-e). On the other hand, if the inverter operates on voltage source without current control in case of a resistive load of 25%, the load voltage is distorted as shown in Fig.23 (a) and (b) except for the proposed models in Fig.23 (c and d) in which voltage output is set to produce a perfect sinusoidal function. The ratio of load consumption and output inverter can affect the amplitude of load voltage. The higher the ratio, the lower the load voltage

amplitude, conforming to the work of Achim Woyte et. al.[8]. The results during islanding phenomena for RLC loads connected in parallel at resonance is shown in Fig.24. It is noticed that the amplitude and frequency of load voltage is kept constant. Therefore, it is difficult to detect islanding by using the passive detection method. However, as compared to the PSpice simulation, the proposed model, which is based on ordinary differential equations, consumes much less for computation time as shown in Table 4. Another advantage of the proposed models is that it does not encounter any convergence problem, which is often the case for PSpice.

Load type	P_{load} (pu.)	PSpice (second)	State space averaged (second)	Piecewise (second)
R	0.25	103	1	6
R	1.0	175	1	5
R	1.25	170	1	5
RLC	1.0	200	1	6

Table 4. Comparison of the time for computation between the PSpice Program and the proposed models

5. Conclusions

The technique to derive a dc-ac full bridge switching converter for a PV grid-connected system are proposed in this paper. An analysis of islanding phenomena due to load variations of R and RLC connections can be easily derived by using the state-space averaging technique and the piecewise technique with feedback current control by setting up the duty cycle with sinusoidal terms around constant value of 0.5. The solution of the two proposed models can be handled via MATLAB/SIMULINK in fast speed and with the absence of the convergence problem, as opposed PSpice simulation. The load voltage behavior simulated by the two proposed models are compared with experiments and the PSpice Program showing good agreement. Small differences, however, were introduced due to parasitic element effects and boundary values of load voltage in the proposed model. Nevertheless, the results demonstrate that a simple and effective model of a grid-connected PV system can be developed. This technique can potentially be further developed for implementation in larger systems consisting of a large array of grid-connected PV modules.

6. Acknowledgements

The authors would like to thank the Joint Graduate School of Energy and Environment (JGSEE), King Mongkut's University of Technology Thonburi (KMUTT) for their kind contribution in providing financial support for this study and the Clean Energy Systems (CES) Group at KMUTT.

7. References

[1] 15 – Year Strategic Plan Promoting New and Renewable Technology Development 15 year (2007-2022), Ministry of Energy, Thailand

[2] Power Development Plan, PDP 2007 Rev 2nd, National Energy Policy Office, Bangkok, 2009
[3] "Renewable Energy Policy: Recent Policies on SPP/VSPP, Seminar on "Renewable Energy: Technology, Markets and Policies in Southeast Asia", BITEC, Bangkok, Thailand, 6 June 2007
[4] PEA/MEA Regulations for the Purchase of Power from Very Small Power Producers (2005)
[5] PEA/MEA Regulations on Uses of Electrical Networks (2008)
[6] PEA/MEA Regulations on Operations of Electrical Networks (2008)
[7] PEA/MEA Regulations on Connections of Electrical Networks (2008)
[8] IEEE929-2000 IEEE Recommended Practice for Utility Interface of Photovoltaic Systems
[9] IEEE 1547.1-2005 Standard Conformance Test Procedures for Equipment Interconnecting Distributed Resources with Electric Power Systems
[10] IEC 62116 Test Procedure of Islanding Prevention Measures for Utility-Interconnected Photovoltaic Inverters
[11] IEC 61727 Photovoltaic Systems- Characteristics of the Utility Interface
[12] Simon S. Ang, Power Switching Converters, Marcel Dekker, 1995
[13] Daniel M. Mitchell, DC-DC Switching Regulator Analysis, McGraw-Hill Book Company, 1988
[14] Muhammad H.Rashid Power Electronics Circuit, Devices and Application, Third Edition, Pearson Education International, 2004
[15] Marian P. Kazmierkowski and Luigi Malesani , Current Control Technique for Three-Phase Voltage-Source PWM Converter: A Survey, IEEE Transactions on Industrial Electronics, Vol. 45,No. 5, pp.691-703(1998)
[16] Chi Kong Tse, Complex Behavior of Switching Power Converter, CRC Press, 2003
[17] Veerapol Monyakul, A New Bidirectional AC-DC Converter with Low Harmonic Input Currents and an Adjustable Power Factor, Doctor of Philosophy Thesis, Oklahoma State University, Stillwater, Oklahoma USA, December,1993
[18] Mei Xu, Roderick V.N Melnik and Uffe Borup, Modeling Anti Islanding Protection Devices for Photovoltaic Systems, Renewable Energy, Vol.26, No.15,pp 2195-2216(2004)
[19] Achim Woyte, Ronnie Belmans and Johan Jijs, Testing the Islanding Protection Function of Photovoltaic Inverters, IEEE Transactions on Energy Conversion Vol.18, No.1, pp. 157-162(2003)

Distributed Generation

Edited by D N Gaonkar

ISBN 978-953-307-046-9
Hard cover, 406 pages
Publisher InTech
Published online 01, February, 2010
Published in print edition February, 2010

In the recent years the electrical power utilities have undergone rapid restructuring process worldwide. Indeed, with deregulation, advancement in technologies and concern about the environmental impacts, competition is particularly fostered in the generation side, thus allowing increased interconnection of generating units to the utility networks. These generating sources are called distributed generators (DG) and defined as the plant which is directly connected to distribution network and is not centrally planned and dispatched. These are also called embedded or dispersed generation units. The rating of the DG systems can vary between few kW to as high as 100 MW. Various new types of distributed generator systems, such as microturbines and fuel cells in addition to the more traditional solar and wind power are creating significant new opportunities for the integration of diverse DG systems to the utility. Interconnection of these generators will offer a number of benefits such as improved reliability, power quality, efficiency, alleviation of system constraints along with the environmental benefits. Unlike centralized power plants, the DG units are directly connected to the distribution system; most often at the customer end. The existing distribution networks are designed and operated in radial configuration with unidirectional power flow from centralized generating station to customers. The increase in interconnection of DG to utility networks can lead to reverse power flow violating fundamental assumption in their design. This creates complexity in operation and control of existing distribution networks and offers many technical challenges for successful introduction of DG systems. Some of the technical issues are islanding of DG, voltage regulation, protection and stability of the network. Some of the solutions to these problems include designing standard interface control for individual DG systems by taking care of their diverse characteristics, finding new ways to/or install and control these DG systems and finding new design for distribution system. DG has much potential to improve distribution system performance. The use of DG strongly contributes to a clean, reliable and cost effective energy for future. This book deals with several aspects of the DG systems such as benefits, issues, technology interconnected operation, performance studies, planning and design. Several authors have contributed to this book aiming to benefit students, researchers, academics, policy makers and professionals. We are indebted to all the people who either directly or indirectly contributed towards the publication of this book.

How to reference

In order to correctly reference this scholarly work, feel free to copy and paste the following:

N. Chayawatto, N.Patcharaprakiti, V. Monyakul, K.Kirtikara and K. Tunlasakun (2010). Distributed Generation and Islanding – Study on Converter Modeling of PV Grid-Connected Systems under Islanding Phenomena, Distributed Generation, D N Gaonkar (Ed.), ISBN: 978-953-307-046-9, InTech, Available from: http://www.intechopen.com/books/distributed-generation/distributed-generation-and-islanding-study-on-converter-modeling-of-pv-grid-connected-systems-under-

INTECH
open science | open minds

InTech Europe
University Campus STeP Ri
Slavka Krautzeka 83/A
51000 Rijeka, Croatia
Phone: +385 (51) 770 447
Fax: +385 (51) 686 166
www.intechopen.com

InTech China
Unit 405, Office Block, Hotel Equatorial Shanghai
No.65, Yan An Road (West), Shanghai, 200040, China
中国上海市延安西路65号上海国际贵都大饭店办公楼405单元
Phone: +86-21-62489820
Fax: +86-21-62489821

IntechOpen